

N-end rule-mediated proteasomal degradation of ATGL promotes lipid storage

Jiesi Xu^{1,*,#}, Zhenglong Liu^{1,2,*}, Jianxin Zhang^{1,2}, Siyu Chen^{1,2}, Wei Wang¹, Xuefan Zhao^{1,2}, Mei Zhen³ and Xun Huang^{1,#}

¹ State Key Laboratory of Molecular and Developmental Biology, Institute of Genetics and Developmental Biology, Chinese Academy of Sciences, Beijing 100101, China

² University of Chinese Academy of Sciences, Beijing 100049, China

³ Lunenfeld and Tanebaum Research Institute; Department of Molecular Genetics, Department of Physiology, University of Toronto, Toronto, Ontario, Canada M5G 1X5

* Equal contribution

To whom correspondence should be addressed at:

State Key Laboratory of Molecular Developmental Biology, Institute of Genetics and Developmental Biology, Chinese Academy of Sciences, Beijing 100101, China

86-10-64806560 (Tel&Fax)

Email: jxu@genetics.ac.cn; xhuang@genetics.ac.cn

Running title: N-end rule regulation of ATGL

Keywords: ATGL, N-end rule pathway, lipid storage, lipolysis, obesity

Highlights:

- Proteasome activity is positively correlated with lipid storage in worm, fly and mammalian cells.
- The N-end rule E3 ligases UBR1 and UBR2 mediate the proteasomal degradation of ATGL and affect lipid storage.
- Mice with knock-in of the N-end rule-resistant ATGL(F2A) exhibit elevated lipolysis, reduced lipid storage, and resistance to high-fat diet (HFD)-induced hepatic steatosis.
- Hepatic UBR1 knockdown attenuates HFD-induced hepatic steatosis and improves glucose tolerance.

Word count: 4446; Number of figures: 6

Abstract

Cellular lipid storage is regulated by the balance of lipogenesis and lipolysis. The rate-limiting triglyceride hydrolase ATGL (desnutrin/PNPLA2) is critical for lipolysis. The control of ATGL transcription, localization and activation has been intensively studied, while regulation of the protein stability of ATGL is much less explored. Here we showed that the protein stability of ATGL is regulated by the N-end rule in cultured cells and in mice. The N-end rule E3 ligases UBR1 and UBR2 reduce the level of ATGL and affect lipid storage. The N-end rule-resistant ATGL(F2A) mutant, in which the N-terminal phenylalanine (F) of ATGL is substituted by alanine (A), has increased protein stability and enhanced lipolysis activity. *ATGL*^{F2A/F2A} knock-in mice are protected against high-fat diet (HFD)-induced obesity, hepatic steatosis and insulin resistance. Hepatic knockdown of *Ubr1* attenuates HFD-induced hepatic steatosis by enhancing the ATGL level. Finally, the protein levels of UBR1 and ATGL are negatively correlated in the adipose tissue of obese mice. Our study reveals N-end rule-mediated proteasomal regulation of ATGL, a finding which may potentially be beneficial for treatment of obesity.

1 **Introduction**

2 Obesity is a major risk factor for common diseases such as nonalcoholic fatty liver
3 disease (NAFLD), cardiovascular diseases, type II diabetes, and some cancers (1). The
4 cause of obesity is complicated, and includes factors such as excessive food intake, lack
5 of physical activity and genetic susceptibility; however, in general, the main reason is
6 excessive lipid storage (2). At the cellular level, the balance of lipogenesis and lipolysis
7 largely determines the lipid storage level. Reduced lipogenesis or elevated lipolysis has
8 often been reported to be protective against the development of obesity and obesity-
9 associated diseases (3; 4).

10 ATGL is a rate-limiting executor of lipolysis and its level or activity has been
11 associated with various metabolic conditions (5-10). Loss-of-function mutations in
12 human ATGL cause neutral lipid storage disease with myopathy (NLSDM) (11). *Atgl*-
13 deficient mice accumulate large amounts of lipid in the heart, which causes cardiac
14 dysfunction and premature death (12). Interestingly, adipose tissue-specific
15 overexpression or deletion of *Atgl* appears to be beneficial. Mice with adipose *ATGL*
16 overexpression were protected from diet-induced obesity and showed improved glucose
17 homeostasis (13). Adipose-specific *Atgl* knockout mice had slightly increased body
18 weight, but exhibited improved glucose tolerance and hepatic insulin sensitivity (14).
19 Pharmacological inhibition of ATGL by Atglistatin has beneficial effects on high-fat
20 diet (HFD)-induced obesity and hepatic steatosis (15). Therefore, the temporal and
21 spatial regulation of ATGL level or activity appear to be critical for determining the
22 physiological outcome.

23 ATGL protein is expressed at low levels in non-adipose tissues, but is highly
24 expressed in white and brown adipose tissue (16). Previous studies revealed that ATGL
25 expression/activity can be regulated transcriptionally and post-transcriptionally (17-21).
26 Numerous binding partners of ATGL have also been identified. ABHD5 (α/β hydrolase

27 domain containing 5, also named CGI58) is a classic cofactor that directly binds to and
28 activates ATGL (19). On the other hand, ATGL activity can be inhibited by GOS2,
29 which physically interacts with the N-terminal patatin domain of ATGL (20). In
30 addition, other ATGL binding partners, such as UBXD8, PEDF, COP1, PEX2 and the
31 Arf1 exchange factor GBF1, may be responsible for modulating the trafficking,
32 localization or protein level of ATGL (18; 22-25). Despite significant advances in our
33 knowledge of the control of ATGL transcription, localization and activation, the
34 complete set of *in vivo* regulatory events for ATGL is far from clear.

35 In this study, we found that ATGL protein level is modulated by the N-end rule
36 pathway E3 ligases UBR1 and UBR2. The N-end rule pathway is a proteolytic system in
37 which certain N-terminal residues of short-lived proteins are recognized by a class of
38 ubiquitin ligases to achieve proteasome-mediated degradation (26). We demonstrated
39 that mice with a knock-in of the N-end rule-resistant mutation ATGL(F2A) (designated
40 as *Atgl*^{F2A/F2A}) exhibit elevated lipolysis and are resistant to HFD-induced obesity and
41 hepatic steatosis.

42

43 **Research design and methods**

44 **Mice**

45 *Atgl*^{F2A/F2A} knock-in mice on the C57BL/6 background were generated by Beijing
46 Biocytogen Co., Ltd. All mice were housed in environmentally controlled conditions
47 (temperature 22°C, 12:12 LD cycle lights on at 0730h). Male mice were used for all
48 experiments. For HFD feeding, 8-week-old *Atgl*^{+/+} and *Atgl*^{F2A/F2A} mice were housed
49 individually and fed an HFD with 60% kcal fat (Research Diets, D12492, New
50 Brunswick) for 16 weeks. Glucose tolerance test (GTT) and insulin sensitivity test (ITT)
51 were performed after 16-weeks of HFD feeding. For hepatic knockdown of *Ubr1*, 8-

52 week-old *Atgl*^{+/+} and *Atgl*^{F2A/F2A} mice were injected intravenously (i.v.) with 3×10¹¹
53 genomic copies (GC) of AAV-TBG-sh*Con* or AAV-TBG-sh*Ubr1* AAVs, followed by
54 feeding with an HFD with 60% kcal fat (Research Diets, D12492) for 8 weeks. All mice
55 were fasted for 5-6 hours prior to euthanasia, except when otherwise indicated. All
56 animal care and treatment procedures were approved by the Institutional Animal Care
57 and Use Committee.

58

59 **Cells and cell culture**

60 HepG2 cells (#HB-8065), HeLa cells (#CCL-2) and 3T3L1 preadipocytes (#CL-173)
61 were purchased from ATCC (Manassas, VA). For transfection, a total of 100 pmol
62 siRNA oligonucleotides were transfected into cells in 6-well plates using Lipofectamine
63 3000 (Invitrogen, Waltham).

64

65 **Adenoviruses and adeno-associated viruses**

66 The coding sequences of human ATGL and the ATGL(F2A) mutant were amplified by
67 PCR and cloned into the adenovirus vector pADV-mCMV-MCS-3×flag. Adenovirus
68 was produced by transfection in 293A cells and purified via the cesium chloride gradient
69 centrifugation method. Adeno-associated virus (AAV) expressing shRNA against mouse
70 *Ubr1* was generated using the AAV vector pAAV-TBG-MCS-3Flag-WPRE. The target
71 sequence is 5'-CCCGTAAGATCCTTCATGA -3'. AAV virus was produced by
72 transfection into 293T cells and purified via discontinuous iodixanol gradient (27). Viral
73 genome titers were determined by qRT-PCR.

74

75 **Statistics**

76 All data are shown as mean ± SEM, except that in Fig. 1D, 2D and 3H, data are shown

77 as violin plots with median. Statistical analyses were performed with the 2-tailed,
78 unpaired Student's *t* test or ANOVA with post-hoc Tukey's multiple comparisons test
79 using GraphPad.

80

81 **Data and Resource**

82 Datasets and resources are available upon request.

83

84 **Results**

85 **Proteasome activity is positively correlated with lipid storage in worm, fly and** 86 **mammalian cells.**

87 In order to find new regulators of neutral lipid storage, we previously performed an
88 RNAi screen in *C. elegans* (28). We found that two proteasome component genes, *pas-5*
89 and *pbs-4*, caused a decreased lipid storage phenotype when knocked down (Fig. 1A,
90 Supplementary Fig. 1A and Supplementary Table S1). We then screened other
91 proteasome components through RNAi. Knockdown of nearly all of the core
92 components and a few regulatory components caused a similar reduced lipid storage
93 phenotype (Supplementary Table S1). This suggests a general requirement for the
94 proteasome for proper lipid storage. Meanwhile, in a genetic screen in *Drosophila* (29),
95 we found that overexpression of the proteasome regulatory subunit Rpn2 dramatically
96 increases lipid storage in *Drosophila* 3rd instar salivary gland (Supplementary Fig. 1B).
97 These findings suggest that proteasome activity promotes lipid storage in worm and fly.

98 We examined the effect of the proteasome inhibitor MG132 on lipid storage in
99 worms and mammalian cells. Compared to the control, MG132 treatment reduced the fat
100 content in worms in a dose-dependent manner (Fig. 1B). Similarly, the size and the
101 number of lipid droplets, as well as triglyceride levels, were all decreased in MG132-
102 treated HepG2 cells (Fig. 1C-F). Together, our results indicate that proteasome activity

103 positively correlates with lipid storage in worm, fly and mammalian cells.

104

105 **The ATGL level is regulated by proteasome activity.**

106 We next explored the mechanism underlying the relationship between inhibition of
107 proteasome activity and decreased lipid storage. The proteasome may be involved in the
108 degradation of a negative regulator of lipogenesis or a positive regulator of lipolysis.
109 Previous work showed that the level of ATGL is increased by proteasome inhibitor
110 treatment (18). Therefore, we analyzed the link between proteasome activity, ATGL
111 level, and lipid storage. MG132 treatment greatly increased the endogenous ATGL level
112 in both normal and OA-loaded cells (Fig. 1G). Interestingly, OA treatment also
113 enhanced the protein levels of ATGL compared to the control (Fig. 1G). To test whether
114 elevated ATGL is responsible for the MG132-mediated inhibition of lipid storage in
115 OA-loaded cells, we knocked down ATGL in HepG2 cells. The reduced lipid storage
116 caused by MG132 treatment was significantly suppressed by knockdown of ATGL (Fig.
117 1C-F, and supplementary Fig. 1C).

118 In agreement with previous finding (18; 24), the level of ubiquitinated ATGL was
119 increased upon MG132 treatment (Fig. 1H). In contrast to MG132, treatment with
120 Bafilomycin A1 (BFA1), a lysosome H⁺-ATPase inhibitor, did not affect endogenous
121 ATGL levels in cells with or without OA treatment (Fig. 1I). This indicates that ATGL
122 is mainly degraded through the ubiquitin-proteasome pathway. Overall, these data
123 suggest that proteasome activity regulates lipid storage, at least partially, through ATGL
124 degradation.

125

126 **The N-end rule pathway ubiquitin ligases UBR1 and UBR2 affect ATGL stability**
127 **and lipid storage in cells.**

128 We next sought to identify the E3 ligase(s) that might be responsible for ATGL

129 ubiquitination and degradation. The candidate E3 ligase should fulfill at least two
130 criteria: first, when mutated, it should have a lipid metabolism-related phenotype *in vivo*;
131 and second, it should affect ATGL ubiquitination. Based on these two criteria, we
132 examined the potential involvement of the N-end rule E3 ligase UBR1 (30). UBR is as
133 an important component of the N-end rule pathway, and it recognizes and binds to
134 proteins bearing destabilizing N-terminal residues, leading to their ubiquitination and
135 subsequent degradation (31). Importantly, ATGL bears a destabilizing N-end residue,
136 phenylalanine (F), and this residue is conserved in vertebrates (Fig. 2A). In addition, a
137 previous report has shown that *Ubr1*^{-/-} mice exhibit reduced adiposity (30).

138 We then examined whether the stability of ATGL is regulated by UBR1. *UBR1*
139 RNAi increased the ATGL protein level compared to the negative control (Fig. 2B).
140 Similarly, the endogenous ATGL protein level was increased in HeLa cells with
141 knockdown of *UBR2*, which belongs to UBR protein family and plays redundant roles
142 (31), and was greatly increased in *UBR1/UBR2* double RNAi cells compared to the
143 control (Fig. 2B). Next, we tested whether UBR1 and UBR2 also affect ATGL-mediated
144 lipolysis. ATGL RNAi led to increased lipid storage (Fig. 2C-F). In contrast,
145 knockdown of *UBR1* or *UBR2* reduced the size and number of lipid droplets and
146 lowered the level of triglyceride accumulation in *ATGL* RNAi HepG2 cells (Fig. 2C-F).
147 This indicates that UBR1 and UBR2 affect ATGL-regulated lipid storage.

148 We also examined the physical interaction between the proteins. Both UBR1 and
149 UBR2 were associated with ATGL-Flag (Fig. 2G-H). We further determined the lysine
150 residue(s) of ATGL that are ubiquitinated by UBR. Consistent with previous findings
151 that the polyubiquitination signal of ATGL is located at the N-terminus of the protein
152 (18; 24), the ubiquitination signal was detected in Flag-tagged full-length ATGL and a
153 Flag-tagged N-terminal fragment (amino acids 1-160) (Fig. 2I and Supplementary Fig.

154 1D). Notably, the ubiquitination signal of both full-length and N-terminal ATGL was
155 considerably decreased upon UBR1 knockdown (Fig. 2I and Supplementary Fig. 1D).
156 We searched for UBR1-dependent ubiquitination sites in the N-terminal patatin domain
157 of ATGL. There are six lysine (K) residues in that region and UBR1 knockdown
158 increased the ATGL protein level when lysine was mutated to arginine (R) at positions
159 68, 74, 78, 92, or 135 (Supplementary Fig. 1E-G). However, the protein and
160 polyubiquitination levels of ATGL(K100R) did not respond to UBR1 knockdown (Fig.
161 2I and Supplementary Fig. 1G), suggesting that K100 is an UBR1-dependent
162 ubiquitination site of ATGL.

163 Since OA treatment also increased ATGL protein levels (Fig. 1G), we next tested
164 whether OA treatment affected the polyubiquitination levels of ATGL. The
165 polyubiquitination levels of ATGL were slightly increased by treatment with OA or
166 lipolytic inducer (Fig. 2J). Moreover, knockdown of UBR1 increased ATGL protein
167 stability with or without OA treatment. Similar patterns were observed following the
168 knockdown of COP1 and PEX2, two E3 ligases for ATGL, except that knockdown of
169 PEX2 failed to decrease the polyubiquitination level of ATGL upon treatment with
170 lipolytic inducer (Supplementary Fig. 2A and B). This may be because lipolysis
171 enhances the protein level of PEX2 (24). In line with this, neither OA treatment nor
172 knockdown of E3 ligases for ATGL significantly affected the polyubiquitination levels
173 of ATGL(K100R) (Supplementary Fig. 2C and D), which provides further evidence that
174 K100 is important for its protein stability. Collectively, these results indicate that the
175 stability of ATGL can be regulated by UBR1 and UBR2.

176

177 **The N-end rule residue affects the stability of ATGL.**

178 To investigate whether the N-terminal phenylalanine residue of ATGL is important for
179 its stability, we compared the stability of wild-type ATGL in HeLa cells with two ATGL

180 mutants, ATGL(F2A) and ATGL(F2V), in which the N-terminal destabilizing residue
181 phenylalanine (F) of ATGL was mutated to the stabilizing residue alanine (A) or valine
182 (V). Western blot results showed that the ATGL(F2A) and ATGL(F2V) mutants are more
183 stable than ATGL(WT) (Fig. 3A-B). We then explored the contribution of the
184 destabilizing phenylalanine residue to the ubiquitination of ATGL. The level of
185 ubiquitinated ATGL(F2A) was lower than that of ATGL(WT) in the presence of MG132
186 (Fig. 3C). Furthermore, knockdown of *UBR1* and *UBR2* enhanced the level of
187 ATGL(WT) protein but not the ATGL(F2A) mutant (Fig. 3D). This suggests that the N-
188 terminal phenylalanine residue of ATGL is important for UBR1- and UBR2-regulated
189 protein stability.

190 ATGL is highly expressed in adipocytes and ATGL-mediated lipolysis is essential
191 for providing free fatty acid (FFA) for energy production during fasting (16). We then
192 tested whether the ATGL(F2A) mutant affects lipolysis and lipid storage in 3T3L1
193 adipocytes. In basal-state 3T3L1 adipocytes, levels of lipolysis, assessed by FFA and
194 glycerol release, were comparable in cells expressing ATGL(WT) and ATGL(F2A),
195 except that glycerol release was increased in ATGL(F2A) cells at 4 hours (Fig. 3E and
196 F). Stimulation of lipolysis with isoproterenol led to increased FFA and glycerol release,
197 and this enhancement was greater in ATGL(F2A) cells compared to ATGL(WT) cells
198 (Fig. 3E and F and Supplementary Fig. 2E). The N-end rule residue substitution did not
199 affect the binding of ATGL with CGI58, an activator of ATGL, or with G0S2, an
200 inhibitor of ATGL (Supplementary Fig. 2F and G). Accordingly, lipid droplet size and
201 number, and triglyceride accumulation were decreased in stimulated ATGL(F2A)-
202 expressing cells compared to ATGL(WT)-expressing cells (Fig. 3G-J). In sum, the N-
203 end rule residue affects the stability of ATGL and the level of ATGL-mediated lipolysis.

204

205 **ATGL(F2A) knock-in mice have elevated lipolysis and FAO in adipose tissue.**

206 We next sought to reveal the effect of stabilized ATGL in mice. We generated mice with
207 knock-in of the ATGL(F2A) mutation, designated as *Atgl*^{F2A/F2A} (Supplementary Fig. 3A
208 and B). Supplementary Table S2 shows the metabolic profiles of *Atgl*^{+/+} and *Atgl*^{F2A/F2A}
209 mice fed on a chow diet.

210 In gonadal white adipose tissue (WAT) and brown adipose tissue (BAT), the ATGL
211 level was increased by 3-fold and 1.5-fold, respectively, in *Atgl*^{F2A/F2A} mice compared to
212 control mice (Fig. 4A and B). Similar to adipose tissue, the ATGL protein level was
213 elevated in muscle from *Atgl*^{F2A/F2A} mice (Supplementary Fig. 3C). Along with the
214 increased protein level, ATGL(F2A) caused enhanced lipolysis *ex vivo* (Fig. 4C and D).
215 When mice were fed an HFD for 8 weeks, ATGL(F2A) led to enhanced FFA release
216 from labeled triglyceride compared to control mice (Fig. 4E).

217 Previous studies reported that overexpression of ATGL leads to activation of
218 PPAR α signaling and fatty acid β -oxidation (FAO) (32; 33). Similarly, expression levels
219 of genes related to PPAR α signaling and FAO were higher in the gonadal WAT from the
220 HFD-fed *Atgl*^{F2A/F2A} mice compared to the control (Fig. 4F). Expression levels of genes
221 involved in lipogenesis and lipolysis were not significantly affected (Fig. 4F). Moreover,
222 direct measurement of FAO using [³H]-palmitate showed that FAO was enhanced in the
223 WAT of HFD-fed *Atgl*^{F2A/F2A} mice (Fig. 4G). The development of obesity is associated
224 with stereotypical changes in adipose tissue expression of inflammatory genes. We then
225 examined the adipose inflammation in HFD-fed mice. The adipose inflammation was
226 not significantly affected in HFD-fed *Atgl*^{F2A/F2A} mice (Supplementary Fig. 3D). Overall,
227 these data suggest that *Atgl*^{F2A/F2A} mice have increased levels of ATGL protein and
228 triglyceride hydrolase activity in adipose tissue.

229

230 ***Atgl*^{F2A/F2A} mice are resistant to diet-induced obesity and hepatic steatosis.**

231 Next, we examined the effect of ATGL(F2A) on the development of obesity. *Atgl*^{+/+} and
232 *Atgl*^{F2A/F2A} mice were pair-fed an HFD for 16 weeks starting from 8 weeks of age. We
233 used pair-feeding to ensure similar food intake by these two groups (Supplementary Fig.
234 3E), because it has been reported that loss of *Atgl* or pharmacological ATGL inhibition
235 affects food intake (15; 34). The plasma parameters are shown in Supplementary Table
236 S3.

237 The body weight gain of *Atgl*^{F2A/F2A} mice was less than that of *Atgl*^{+/+} mice (Fig.
238 5A). Glucose tolerance and insulin sensitivity were improved in HFD-fed *Atgl*^{F2A/F2A}
239 mice compared to *Atgl*^{+/+} mice (Fig. 5B-D). To determine the effect of ATGL(F2A) on
240 energy balance, we measured oxygen consumption (O₂), carbon dioxide (CO₂)
241 production and energy expenditure. Their levels were higher in HFD-fed *Atgl*^{F2A/F2A}
242 mice compared to *Atgl*^{+/+} mice (Fig. 5E and F, Supplementary Fig. 3F and G).

243 The attenuated body weight gain in HFD-fed *Atgl*^{F2A/F2A} mice led us to examine
244 adiposity. The liver weight and the weights of WAT and BAT were decreased in
245 *Atgl*^{F2A/F2A} mice compared to *Atgl*^{+/+} mice when fed an HFD (Fig. 5G, and
246 Supplementary Fig. 3H). The sizes of adipocytes in WAT and BAT were also decreased
247 in adipose tissue sections from HFD-fed *Atgl*^{F2A/F2A} mice compared to control mice (Fig.
248 5H-J).

249 The reduced liver weight in HFD-fed *Atgl*^{F2A/F2A} mice led us to further analyze the
250 effect of ATGL(F2A) in liver. Hepatic triglyceride and total cholesterol levels, and
251 hepatic lipid droplet accumulation were significantly decreased in HFD-fed *Atgl*^{F2A/F2A}
252 mice compared to *Atgl*^{+/+} mice (Fig. 5K and L). The ALT level, which indicates liver
253 damage, was decreased in HFD-fed *Atgl*^{F2A/F2A} mice compared to *Atgl*^{+/+} mice (Fig. 5M).
254 ATGL protein levels were increased in the liver of *Atgl*^{F2A/F2A} mice compared to control
255 mice (Supplementary Fig. 3I). To further determine whether reduced lipid accumulation

256 in the liver of *Atgl*^{F2A/F2A} mice was attributable to enhanced lipid degradation, we
257 measured the FAO level. Expression levels of genes involved in FAO and fatty acid
258 transport were significantly increased (Fig. 5N). The FAO level was significantly
259 enhanced in the liver of HFD-fed *Atgl*^{F2A/F2A} mice compared to control (Fig. 5O). Taken
260 together, these results suggest that *Atgl*^{F2A/F2A} mice, which carry a stabilizing N-terminal
261 amino acid substitution, are resistant to HFD-induced obesity and hepatic steatosis.

262

263 **Hepatic knockdown of *Ubr1* suppresses HFD-induced fatty liver.**

264 We then examined the physiological effect of UBR1-mediated ATGL degradation in
265 mice. We knocked down *Ubr-1* (AAV-TBG-sh*Ubr1*) in the liver of *Atgl*^{+/+} or *Atgl*^{F2A/F2A}
266 mice. The TBG (thyroxine binding globulin) promoter ensures gene knockdown in the
267 liver. Control animals received AAV-TBG-sh*Con*. Hepatic knockdown of *Ubr1* did not
268 affect hepatic triglyceride levels in fed or fasted mice on a chow diet (Supplementary
269 Fig. 4A). We also fed the animals with an HFD for 8 weeks. As expected, HFD-fed
270 *Atgl*^{F2A/F2A} mice showed attenuated body weight gain, less hepatic lipid accumulation,
271 and decreased plasma ALT levels compared to HFD-fed *Atgl*^{+/+} mice (Fig. 6A-C and
272 Supplementary Fig. 4B). These beneficial effects were not affected by hepatic
273 knockdown of *Ubr1* in HFD-fed *Atgl*^{F2A/F2A} mice (Fig. 6A-C and Supplementary Fig.
274 4B), which suggests that UBR1-mediated ATGL degradation is blunted in *Atgl*^{F2A/F2A}
275 mice. Nevertheless, hepatic knockdown of *Ubr1* caused reductions in hepatic lipid
276 accumulation and plasma ALT levels in HFD-fed *Atgl*^{+/+} mice (Fig. 6A-C and
277 Supplementary Fig. 4B).

278 We then tested the energy balance and glucose homeostasis in HFD-fed *Atgl*^{+/+} and
279 *Atgl*^{F2A/F2A} mice with or without knockdown of hepatic *Ubr1*. The VO₂, VCO₂ and
280 energy expenditure were significantly enhanced in *Atgl*^{F2A/F2A} mice compared to *Atgl*^{+/+}

281 mice (Supplementary Fig. 4C-E). Knockdown of *Ubr1* did not affect their levels
282 irrespective of genotypes (Supplementary Fig. 4C-E). In line with previous findings,
283 HFD-fed *Atgl*^{F2A/F2A} mice showed improved glucose homeostasis and insulin sensitivity
284 compared to *Atgl*^{+/+} mice (Fig. 6D-F, Supplementary Fig. 4F). Although knockdown of
285 *Ubr1* improved glucose homeostasis in AAV-TBG-sh*Ubr1*-treated *Atgl*^{+/+} mice
286 compared to AAV-TBG-sh*Con* treated *Atgl*^{+/+} mice, it had no effects on glucose
287 homeostasis in *Atgl*^{F2A/F2A} mice (Fig. 6D-F and Supplementary Fig. 4F). To examine the
288 activity of the insulin pathway, HFD-fed *Atgl*^{+/+} and *Atgl*^{F2A/F2A} mice were injected with
289 1 U/kg insulin intraperitoneally. p-AKT(Ser 473) and p-AKT(Thr 308) levels were
290 enhanced in the liver of *Atgl*^{F2A/F2A} mice compared to *Atgl*^{+/+} mice (Fig. 6G).
291 Importantly, knockdown of hepatic *Ubr1* did not affect the activity of the insulin
292 pathway in the liver of *Atgl*^{F2A/F2A} mice (Fig. 6G). Moreover, knockdown of hepatic
293 *Ubr1* did not affect the activity of the insulin pathway in the muscle and WAT in both
294 genotypes (Supplementary Fig. G-H). Taken together, these data suggest that the
295 beneficial effects of the *Atgl*^{F2A} mutation on HFD-induced hepatic steatosis and glucose
296 homeostasis in mice are not affected by knockdown of hepatic *Ubr1*.

297 Analysis of hepatic gene expression levels showed that *Ubr1* deficiency
298 downregulated the expression of *Pparg* and its target *Fabp4* in *Atgl*^{+/+} mice, but this
299 effect was blunted in *Atgl*^{F2A/F2A} mice (Fig. 6H). A similar pattern was shown by other
300 genes involved in lipogenesis (Supplementary Fig. 4I). The expression levels of genes
301 involved in FAO and lipolysis were enhanced in *Atgl*^{F2A/F2A} mice compared to *Atgl*^{+/+}
302 mice (Fig. 6H and Supplementary Fig. 4I). Knockdown of *Ubr1* also increased the
303 expression levels of FAO genes in *Atgl*^{+/+} mice, but it caused no further upregulation of
304 these genes in *Atgl*^{F2A/F2A} mice (Fig. 6H and Supplementary Fig. 4I). Next, we tested
305 whether UBR1 regulates ATGL levels *in vivo*. ATGL protein levels were elevated by

306 knockdown of *Ubr1* in *Atgl^{+/+}* mice, and were not affected by knockdown of *Ubr1* in
307 *Atgl^{F2A/F2A}* mice (Fig. 6I). Accordingly, the polyubiquitination levels of ATGL were
308 lowered by knockdown of hepatic *Ubr1* in *Atgl^{+/+}* mice (Fig. 6J). PNPLA3 and
309 PNPLA4, which are PNPLA family members, also contain N-terminal destabilized
310 residues. PNPLA4 but not PNPLA3 was regulated by UBR1 in HeLa cells
311 (Supplementary Fig. 4J-K). Together, these data suggest that in the HFD condition,
312 hepatic knockdown of *Ubr1* reduces lipogenesis and increases FAO. Moreover, the
313 phenotypic similarity of *Atgl^{F2A/F2A}* mice with or without *Ubr1* knockdown indicates that
314 the N-end rule-mediated degradation of ATGL by UBR1 occurs *in vivo*.

315 We further examined the correlation between UBR1 and ATGL levels in obese
316 mice. Consistent with previous reports, ATGL protein levels were downregulated in
317 *ob/ob* mice. Interestingly, UBR1 levels were upregulated in *ob/ob* mice, which suggests
318 a negative correlation between UBR1 and ATGL levels (Fig. 6K). Together, these
319 results demonstrate that the N-end rule-mediated proteasomal degradation of ATGL
320 regulates hepatic lipid metabolism and insulin sensitivity.

321

322 **Discussion**

323 In this study, we found that ATGL, which possesses a typical destabilizing N-terminal
324 residue, is regulated through the N-end rule pathway. Knockdown of the E3 ligases
325 *UBR1* and *UBR2*, or treatment with a proteasome inhibitor, elevates the ATGL level and
326 reduces lipid storage. Importantly, stabilized ATGL (ATGL(F2A)) has beneficial effects
327 on HFD-induced obesity and associated hepatic steatosis in mice.

328

329 **The N-end rule UBR ligase regulates lipid storage through ATGL.**

330 Based on our results and previous findings (18; 24), inhibition of proteasome activity or

331 RNAi of proteasome components results in reduced lipid storage in *C. elegans*,
332 *Drosophila* and cultured mammalian cells. The proteasomal regulation of lipid storage
333 occurs at least partially through ATGL degradation. Previous studies on ATGL protein
334 levels used N-terminal tagged ATGL, thus possibly masking the N-end rule regulation
335 of this protein (18; 25). The N-end rule regulation of ATGL is apparently not the only
336 mechanism that regulates ubiquitination or degradation of ATGL because the
337 ATGL(F2A) protein can still be ubiquitinated (Fig. 3C). E3 ubiquitin ligase COP1 and
338 PEX2 also target ATGL for proteasomal degradation (18; 24).

339 Our study showed that knockdown of UBR or treatment with proteasome inhibitor
340 can reduce lipid storage in the absence of ATGL in OA-loaded HepG2 cells (Fig. 1C-F,
341 Fig. 2C-F). This suggests that other factors involved in lipolysis or lipogenesis can also
342 be involved in UBR1- or proteasome inhibitor-mediated lipid metabolism. In fact,
343 UBR1 has been shown to degrade lipid droplet proteins in yeast (35). A recent study
344 identified PLIN2 as a substrate of UBR1 in mice (36). This work also showed that liver-
345 specific knockdown of both *Ubr1* and *Ubr2* led to hepatic steatosis in mice fed with an
346 HFD for only 2 weeks. The discrepancy may be due to the different length of HFD
347 treatment. We used 8-week HFD feeding and the hepatic steatosis was prominent in
348 wild-type mice.

349

350 **Beneficial effects of *Atgl*^{F2A/F2A}.**

351 The *Atgl*^{F2A/F2A} mice reported here presumably represent a whole-body gain of function
352 of ATGL. These mice also provide us with an opportunity to study the relationship
353 between ATGL protein stability and organismal physiological function. *Atgl*^{F2A/F2A} mice
354 show improved GTT and ITT results, elevated energy expenditure when fed an HFD,
355 and resistance to HFD-induced obesity and hepatic steatosis. These beneficial effects
356 appear similar to those in *G0S2*^{-/-} and adipose-specific ATGL overexpression (*ap2*-

357 *desnutrin*) mice (13; 37). The common features among these mouse models are elevated
358 lipolysis in adipose tissue and reduced triglyceride accumulation in liver upon HFD
359 feeding.

360 The elevated flux of fatty acids from adipose tissue can result in triglyceride
361 accumulation in other peripheral tissues, such as liver. The decreased triglyceride
362 accumulation in the liver in HFD-fed *Atgl*^{F2A/F2A} mice may be due to decreased FFA
363 release from adipose tissue or increased triglyceride degradation in liver. Although the
364 ATGL level is apparently enhanced in the adipose tissue of *Atgl*^{F2A/F2A} mice, the change
365 of plasma FFA level is modest upon HFD feeding (Fig. 4A and Supplementary Table
366 S3). The enhanced FAO and PPAR α signaling in the adipose tissue of *Atgl*^{F2A/F2A} mice
367 may dampen the FFA release from adipose tissue (Fig. 4F-G). Similarly, plasma FFA
368 levels were only slightly higher in *ap2-desnutrin* mice compared to control mice, which
369 was in part due to elevated FAO within adipose tissue (13). On the other hand, elevated
370 hepatic ATGL levels and enhanced FAO in the liver of *Atgl*^{F2A/F2A} mice may account for
371 attenuated HFD-induced hepatic steatosis. In addition, enhanced energy expenditure,
372 improved insulin sensitivity and attenuated HFD-induced body weight gain may also
373 contribute to the beneficial effect in the liver.

374 Glucose tolerance and insulin sensitivity are improved in HFD-fed *Atgl*^{F2A/F2A} mice.
375 It has been reported that lipotoxicity is a causal factor for insulin resistance. It is
376 plausible that reduced lipid accumulation in liver and decreased adiposity relieve the
377 burden of HFD-induced lipid overload, thus improving glucose tolerance and insulin
378 sensitivity. In line with that, both *G0S2*^{-/-} and *ap2-desnutrin* mice showed improved
379 glucose homeostasis upon HFD feeding. Notably, the beneficial effect in *G0S2*^{-/-} and
380 *Atgl*^{F2A/F2A} mice results from the action of ATGL in both liver and adipose tissue, while
381 the beneficial effect in *ap2-desnutrin* mice is predominantly due to the action of ATGL
382 in adipose tissue. Interestingly, knockdown of hepatic *Ubr1* improved the activity of the

383 insulin pathway (Fig. 6D-F). UBR1 may directly regulate components of the insulin
384 signaling pathway. Alternatively, it may regulate hepatic lipids, such as DAG or
385 ceramide, which in turn affect hepatic insulin signaling.

386

387 **Both loss of function and gain of function of ATGL can yield beneficial**
388 **physiological outcomes.**

389 ATGL apparently has dual effects on metabolism and physiology. Tissue-specific
390 knockout or overexpression of ATGL appears to have beneficial effects in mice (10; 13;
391 14; 38; 39). The same conclusion can be extended to humans. On one hand, loss of
392 ATGL results in NLSM with life-threatening myopathy (11). On the other hand, gain of
393 ATGL function in patients with a C-terminal mutation in PLIN1 is associated with a
394 dominant partial lipodystrophy with severe dyslipidemia, and insulin-resistance (40).
395 We cannot rule out the possibility that the deleterious effects in patients with the PLIN1
396 C-terminal truncation could be caused by a combination of both gain of function of
397 ATGL and partial loss of function of PLIN1. Nevertheless, these results indicate that
398 maintaining a suitable level of ATGL *in vivo* appears to be essential for sustaining
399 healthy physiological conditions in humans. In summary, our findings suggest that the
400 level and the site of ATGL up-regulation are probably critical to determining the
401 outcomes of ATGL manipulation.

402

403 **Conflict of interests**

404 The authors have declared that no conflict of interests exist.

405

406 **Author contributions**

407 J. Xu, Z. Liu, W. Wang, J. Zhang and S. Chen conducted the experiments and analyzed

408 the data. Z. Liu contributed to *C. elegans* experiments. J. Xu and Z. Liu contributed to
409 cell experiments. J. Xu, Z. Liu, J. Zhang, S. Chen and X. Zhao contributed to mouse
410 experiments. W. Wang contributed to western blotting. M. Zhen contributed to the
411 identification of UBR1. J. Xu, Z. Liu and X. Huang wrote the paper.

412

413 **Acknowledgements**

414 We thank Drs. H. Yang, J. Liu, C. Yang, J. Speakman, S. Bao and Z. Xu for providing
415 reagents and helpful discussions. This research was supported by grants 3223000137,
416 9195420001 and 2018YFA0506902 from the National Natural Science Foundation of
417 China and the Ministry of Science and Technology of China. Dr. Huang is the guarantor
418 of this work, had full access to all the data, and takes full responsibility for the integrity
419 of data and the accuracy of data analysis.

420

421 **References**

- 422 1. Tiniakos DG, Vos MB, Brunt EM: Nonalcoholic fatty liver disease: pathology and
423 pathogenesis. *Annual Review of Pathology-Mechanisms of Disease* 2010;5:145-171
- 424 2. Adams JP, Murphy PG: Obesity in anaesthesia and intensive care. *Brit J Anaesth* 2000;85:91-
425 108
- 426 3. Li JJ, Ferry RJ, Diao SY, Xue BZ, Bahouth SW, Liao FF: Nedd4 haploinsufficient mice
427 display moderate insulin resistance, enhanced lipolysis, and protection against high-fat diet-
428 induced obesity. *Endocrinology* 2015;156:1283-1291
- 429 4. Lodhi IJ, Yin L, Jensen-Urstad APL, Funai K, Coleman T, Baird JH, El Ramahi MK, Razani
430 B, Song HW, Fong FH, Turk J, Semenkovich CF: Inhibiting adipose tissue lipogenesis
431 reprograms thermogenesis and PPAR gamma activation to decrease diet-induced obesity. *Cell*
432 *Metab* 2012;16:189-201
- 433 5. Jenkins CM, Mancuso DJ, Yan W, Sims HF, Gibson B, Gross RW: Identification, cloning,
434 expression, and purification of three novel human calcium-independent phospholipase A2 family
435 members possessing triacylglycerol lipase and acylglycerol transacylase activities. *J Biol Chem*
436 2004;279:48968-48975
- 437 6. Villena JA, Roy S, Sarkadi-Nagy E, Kim KH, Sul HS: Desnutrin, an adipocyte gene encoding
438 a novel patatin domain-containing protein, is induced by fasting and glucocorticoids. *J Biol*
439 *Chem* 2004;279:47066-47075
- 440 7. Zimmermann R, Strauss JG, Haemmerle G, Schoiswohl G, Birner-Gruenberger R, Riederer
441 M, Lass A, Neuberger G, Eisenhaber F, Hermetter A, Zechner R: Fat mobilization in adipose
442 tissue is promoted by adipose triglyceride lipase. *Science* 2004;306:1383-1386
- 443 8. Kienesberger PC, Puliniikunnil T, Nagendran J, Young ME, Bogner-Strauss JG, Hackl H,
444 Khadour R, Heydari E, Haemmerle G, Zechner R, Kershaw EE, Dyck JR: Early structural and
445 metabolic cardiac remodelling in response to inducible adipose triglyceride lipase ablation.
446 *Cardiovasc Res* 2013;99:442-451
- 447 9. Kienesberger PC, Puliniikunnil T, Sung MMY, Nagendran J, Haemmerle G, Kershaw EE,

448 Young ME, Light PE, Oudit GY, Zechner R, Dyck JRB: Myocardial ATGL Overexpression
449 decreases the reliance on fatty acid oxidation and protects against pressure overload-induced
450 cardiac dysfunction. *Mol Cell Biol* 2012;32:740-750

451 10. Wu JW, Wang SP, Alvarez F, Casavant S, Gauthier N, Abed L, Soni KG, Yang GS, Mitchell
452 GA: Deficiency of liver adipose triglyceride lipase in mice causes progressive hepatic steatosis.
453 *Hepatology* 2011;54:122-132

454 11. Fischer J, Lefevre C, Morava E, Mussini JM, Laforet P, Negre-Salvayre A, Lathrop M,
455 Salvayre R: The gene encoding adipose triglyceride lipase (PNPLA2) is mutated in neutral lipid
456 storage disease with myopathy. *Nat Genet* 2007;39:28-30

457 12. Haemmerle G, Lass A, Zimmermann R, Gorkiewicz G, Meyer C, Rozman J, Heldmaier G,
458 Maier R, Theussl C, Eder S, Kratky D, Wagner EF, Klingenspor M, Hoefler G, Zechner R:
459 Defective lipolysis and altered energy metabolism in mice lacking adipose triglyceride lipase.
460 *Science* 2006;312:734-737

461 13. Ahmadian M, Duncan RE, Varady KA, Frasson D, Hellerstein MK, Birkenfeld AL, Samuel
462 VT, Shulman GI, Wang YH, Kang CH, Sul HS: Adipose overexpression of desnutrin promotes
463 fatty acid use and attenuates diet-induced obesity. *Diabetes* 2009;58:855-866

464 14. Schoiswohl G, Stefanovic-Racic M, Menke MN, Wills RC, Surlow BA, Basantani MK,
465 Sitnick MT, Cai LZ, Yazbeck CF, Stolz DB, Pulini Kunnil T, O'Doherty RM, Kershaw EE:
466 Impact of reduced ATGL-mediated adipocyte lipolysis on obesity-associated insulin resistance
467 and inflammation in male mice. *Endocrinology* 2015;156:3610-3624

468 15. Schweiger M, Romauch M, Schreiber R, Grabner GF, Hutter S, Kotzbeck P, Benedikt P,
469 Eichmann TO, Yamada S, Knittelfelder O, Diwoky C, Doler C, Mayer N, De Cecco W,
470 Breinbauer R, Zimmermann R, Zechner R: Pharmacological inhibition of adipose triglyceride
471 lipase corrects high-fat diet-induced insulin resistance and hepatosteatosis in mice (vol 8, 14859,
472 2017). *Nature Communications* 2017;8

473 16. Schreiber R, Xie H, Schweiger M: Of mice and men: The physiological role of adipose
474 triglyceride lipase (ATGL). *Bba-Mol Cell Biol L* 2019;1864:880-899

475 17. Ahmadian M, Abbott MJ, Tang TY, Hudak CSS, Kim Y, Bruss M, Hellerstein MK, Lee HY,
476 Samuel VT, Shulman GI, Wang YH, Duncan RE, Kang C, Sul HS: Desnutrin/ATGL is
477 regulated by AMPK and is required for a brown adipose phenotype. *Cell Metab* 2011;13:739-
478 748

479 18. Ghosh M, Niyogi S, Bhattacharyya M, Adak M, Nayak DK, Chakrabarti S, Chakrabarti P:
480 Ubiquitin ligase COP1 controls hepatic fat metabolism by targeting ATGL for degradation.
481 *Diabetes* 2016;65:3561-3572

482 19. Lass A, Zimmermann R, Haemmerle G, Riederer M, Schoiswohl G, Schweiger M,
483 Kienesberger P, Strauss JG, Gorkiewicz G, Zechner R: Adipose triglyceride lipase-mediated
484 lipolysis of cellular fat stores is activated by CGI-58 and defective in Chanarin-Dorfman
485 Syndrome. *Cell Metab* 2006;3:309-319

486 20. Yang XY, Lu X, Lombes M, Rha GB, Chi YI, Guerin TM, Smart EJ, Liu J: The G(0)/G(1)
487 switch gene 2 regulates adipose lipolysis through association with adipose triglyceride lipase.
488 *Cell Metab* 2010;11:194-205

489 21. Roy D, Farabaugh KT, Wu J, Charrier A, Smas C, Hatzoglou M, Thirumurugan K, Buchner
490 DA: Coordinated transcriptional control of adipocyte triglyceride lipase (Atgl) by transcription
491 factors Sp1 and peroxisome proliferator-activated receptor gamma (PPARgamma) during
492 adipocyte differentiation. *J Biol Chem* 2017;292:14827-14835

493 22. Ellong EN, Soni KG, Bui QT, Sougrat R, Golinelli-Cohen MP, Jackson CL: Interaction
494 between the triglyceride lipase ATGL and the Arf1 Activator GBF1. *Plos One* 2011;6

495 23. Olzmann JA, Richter CM, Kopito RR: Spatial regulation of UBXD8 and p97/VCP controls
496 ATGL-mediated lipid droplet turnover. *P Natl Acad Sci USA* 2013;110:1345-1350

497 24. Ding LG, Sun WF, Balaz M, He AY, Klug M, Wieland S, Caiazzo R, Raverdy V, Pattou F,
498 Lefebvre P, Lodhi IJ, Staels B, Heim M, Wolfrum C: Peroxisomal beta-oxidation acts as a
499 sensor for intracellular fatty acids and regulates lipolysis. *Nat Metab* 2021;3:1648-1661

500 25. Niyogi S, Ghosh M, Adak M, Chakrabarti P: PEDF promotes nuclear degradation of ATGL
501 through COP1. *Biochem Biophys Res Commun* 2019;512:806-811

502 26. Bachmair A, Finley D, Varshavsky A: In vivo half-life of a protein is a function of its amino-

503 terminal residue. *Science* 1986;234:179-186

504 27. Zolotukhin S, Byrne BJ, Mason E, Zolotukhin I, Potter M, Chesnut K, Summerford C,
505 Samulski RJ, Muzyczka N: Recombinant adeno-associated virus purification using novel
506 methods improves infectious titer and yield. *Gene Ther* 1999;6:973-985

507 28. Liu ZL, Li X, Ge QL, Ding M, Huang X: A Lipid Droplet-Associated GFP Reporter-Based
508 Screen Identifies New Fat Storage Regulators in *C. elegans*. *J Genet Genomics* 2014;41:305-313

509 29. Yao Y, Li X, Wang W, Liu ZH, Chen JM, Ding M, Huang X: MRT, Functioning with
510 NURF complex, regulates lipid droplet size. *Cell Rep* 2018;24:2972-2984

511 30. Kwon YT, Xia ZX, Davydov IV, Lecker SH, Varshavsky A: Construction and analysis of
512 mouse strains lacking the ubiquitin ligase UBR1 (E3 alpha) of the N-end rule pathway. *Mol Cell*
513 *Biol* 2001;21:8007-8021

514 31. Tasaki T, Sriram SM, Park KS, Kwon YT: The N-End Rule Pathway. *Annu Rev Biochem*
515 2012;81:261-289

516 32. Ong KT, Mashek MT, Bu SY, Greenberg AS, Mashek DG: Adipose triglyceride lipase is a
517 major hepatic lipase that regulates triacylglycerol turnover and fatty acid signaling and
518 partitioning. *Hepatology* 2011;53:116-126

519 33. Haemmerle G, Moustafa T, Woelkart G, Buttner S, Schmidt A, van de Weijer T, Hesselink
520 M, Jaeger D, Kienesberger PC, Zierler K, Schreiber R, Eichmann T, Kolb D, Kotzbeck P,
521 Schweiger M, Kumari M, Eder S, Schoiswohl G, Wongsiriroj N, Pollak NM, Radner FPW,
522 Preiss-Landl K, Kolbe T, Rulicke T, Pieske B, Trauner M, Lass A, Zimmermann R, Hoefler G,
523 Cinti S, Kershaw EE, Schrauwen P, Madeo F, Mayer B, Zechner R: ATGL-mediated fat
524 catabolism regulates cardiac mitochondrial function via PPAR-alpha and PGC-1. *Nature*
525 *Medicine* 2011;17:1076-U1082

526 34. Wu JW, Wang SP, Casavant S, Moreau A, Yang GS, Mitchell GA: Fasting energy
527 homeostasis in mice with adipose deficiency of desnutrin/adipose triglyceride lipase.
528 *Endocrinology* 2012;153:2198-2207

529 35. Ruggiano A, Mora G, Buxo L, Carvalho P: Spatial control of lipid droplet proteins by the
530 ERAD ubiquitin ligase Doa10. *Embo J* 2016;35:1644-1655

531 36. Zhang Y, Lin S, Peng J, Liang X, Yang Q, Bai X, Li Y, Li J, Dong W, Wang Y, Huang Y,
532 Pei Y, Guo J, Zhao W, Zhang Z, Liu M, Zhu AJ: Amelioration of hepatic steatosis by dietary
533 essential amino acid-induced ubiquitination. *Mol Cell* 2022;

534 37. Zhang X, Xie X, Heckmann BL, Saarinen AM, Czyzyk TA, Liu J: Targeted disruption of
535 G0/G1 switch gene 2 enhances adipose lipolysis, alters hepatic energy balance, and alleviates
536 high-fat diet-induced liver steatosis. *Diabetes* 2014;63:934-946

537 38. Reid BN, Ables GP, Otlivanchik OA, Schoiswohl G, Zechner R, Blaner WS, Goldberg IJ,
538 Schwabe RF, Chua SC, Huang LS: Hepatic overexpression of hormone-sensitive lipase and
539 adipose triglyceride lipase promotes fatty acid oxidation, stimulates direct release of free fatty
540 acids, and ameliorates steatosis. *J Biol Chem* 2008;283:13087-13099

541 39. Schreiber R, Hofer P, Taschler U, Voshol PJ, Rechberger GN, Kotzbeck P, Jaeger D, Preiss-
542 Landl K, Lord CC, Brown JM, Haemmerle G, Zimmermann R, Vidal-Puig A, Zechner R:
543 Hypophagia and metabolic adaptations in mice with defective ATGL-mediated lipolysis cause
544 resistance to HFD-induced obesity. *P Natl Acad Sci USA* 2015;112:13850-13855

545 40. Gandotra S, Le Dour C, Bottomley W, Cervera P, Giral P, Reznik Y, Charpentier G, Auclair
546 M, Delepine M, Barroso I, Semple RK, Lathrop M, Lascols O, Capeau J, O'Rahilly S, Magre J,
547 Savage DB, Vigouroux C: Perilipin deficiency and autosomal dominant partial lipodystrophy. *N*
548 *Engl J Med* 2011;364:740-748

549

550 **Figure legends**

551 **Figure 1. ATGL is degraded through the ubiquitin-proteasome system.**

552 (A) BODIPY staining for lipid droplets in *C. elegans* treated by *pas-5* RNAi compared
553 to the N2 control. Scale bar represents 40 μ m. (B) Oil Red O staining for lipid droplets

554 in *C. elegans* treated with the indicated concentration of MG132 for 48 hours. Scale bar
555 represents 40 μm . (C) BODIPY staining for lipid droplets in HepG2 cells transfected with
556 siRNA control or siATGL overnight, then treated with 300 μM oleic acid (OA) with or without
557 60 μM MG132 for 24 hours. Scale bar represents 25 μm . (D) Quantifications of lipid
558 droplet sizes in *C.* N=300 lipid droplets per group. (E) Quantifications of the number of
559 lipid droplets in *C.* N=50 cells per group. (F) Quantifications of TAG levels in *C.* N=3 per
560 group. (G) Western blot analysis of lysates of HeLa cells treated with or without OA,
561 followed by MG132 treatment for the indicated time. (H) Western blot analysis of
562 lysates of HeLa cells transfected with Mock or ATGL-Flag, and treated with MG132 at
563 the indicated concentration. (I) Western blot analysis of lysates of HeLa cells treated
564 with the lysosome inhibitor BFA1 under both normal and OA-loaded conditions. All data
565 are presented as mean \pm SEM, except for the violin plots in D in which the horizontal lines
566 indicate the median. * $p < 0.05$, ** $p < 0.01$, **** $p < 0.0001$.

567

568 **Figure 2. The N-end rule pathway ubiquitin ligases UBR1 and UBR2 regulate**
569 **ATGL stability and lipid storage in cultured cells.**

570 (A) The conserved destabilizing phenylalanine (F) residue at the N-terminus of ATGL
571 (*H.s.*, human; *R.n.*, rat; *M.m.*, mouse; *B.t.*, cattle; *G.g.*, chicken). (B) Western blot
572 analysis of proteins in HeLa cells transfected with control siRNA, siUBR1, siUBR2 or
573 both for 48 hours. (C) BODIPY staining for lipid droplets in HepG2 cells transfected with
574 control siRNA, siUBR1, siUBR2, siATGL, siUBR1+siATGL, and siUBR2+siATGL, and
575 treated with 100 μM OA overnight. Scale bar represents 25 μm . (D) Quantifications of
576 lipid droplet sizes in *C.* N=300 lipid droplets per group. (E) Quantifications of the number
577 of lipid droplets in *C.* N=50 cells per group. (F) Quantifications of triglyceride (TAG)
578 levels in *C.* N=3 per group. (G, H) Immunoprecipitation with anti-Flag antibody and
579 western blot analysis for UBR1 (G), UBR2 (H) and ATGL in HeLa cells transfected with

580 control vector or ATGL-Flag. (I) Immunoprecipitation with anti-Flag antibody and
581 western blot analysis for ubiquitin in HeLa cells transfected with the indicated siRNA and
582 ATGL-Flag or ATGL(K100R)-Flag vector, followed by treatment with MG132. (J)
583 Immunoprecipitation with anti-Flag antibody and western blot analysis for ubiquitin in
584 HeLa cells transfected with the indicated siRNA and ATGL-Flag vector, followed by
585 treatment with or without 100 μ M OA for 16 hours or with 100 μ M OA for 16 hours
586 followed by ISO (0.25 mM IBMX/1 μ M isoproterenol) for 8 hours. All data are presented
587 as mean \pm SEM, except for D (violin plots) in which the horizontal lines indicate the median.
588 * p < 0.05, ** p < 0.01, *** p < 0.001, **** p < 0.0001.

589

590 **Figure 3. The N-end rule residue affects the stability of ATGL and ATGL-mediated**
591 **lipolysis.**

592 (A) Western blot analysis of proteins in HeLa cells transfected with ATGL(WT)-Flag,
593 ATGL(F2A)-Flag or ATGL(F2V)-Flag and treated with 10 μ g/mL cycloheximide for
594 the indicated times. (B) Quantification of relative protein levels in (A). (C)
595 Immunoprecipitation with anti-Flag antibody and western blot analysis for ubiquitin and
596 ATGL-Flag in HeLa cells transfected with ATGL(WT)-Flag and ATGL(F2A)-Flag and
597 treated with or without MG132. (D) Western blot analysis of proteins in HeLa cells
598 stably overexpressing ATGL-Flag or ATGL(F2A)-Flag and transfected with control
599 siRNA or si*UBR1*+si*UBR2* for 48 hours. (E, F) Release of FFA (E) and glycerol (F)
600 from differentiated 3T3L1 adipocytes infected with equal amounts of Ad-ATGL-Flag or
601 Ad-ATGL(F2A)-Flag and treated with or without 10 μ M isoproterenol at 37°C (N=3 per
602 group). (G) BODIPY staining for lipid droplets in differentiated 3T3L1 adipocytes
603 infected with equal amounts of Ad-ATGL-Flag or Ad-ATGL(F2A)-Flag and stimulated
604 with or without 10 μ M isoproterenol for 3 hours. Adipocytes are outlined with dashed
605 yellow lines. Scale bar represents 25 μ m. (H) Quantifications of lipid droplet sizes in G.

606 N=300 lipid droplets per group. (I) Quantifications of the number of lipid droplets in G.
607 N=50 cells per group. (J) Quantifications of TAG levels in G. N=3 per group. All data are
608 presented as mean±SEM, except for H in which the horizontal lines indicate the median. *p
609 < 0.05, **p < 0.01, ***p < 0.001, ****p < 0.0001.

610

611 **Figure 4. *Atgl*^{F2A/F2A} mice have elevated lipolysis in adipose tissue.**

612 (A) Western blot analysis of proteins in the gonadal WAT or BAT from chow diet-fed
613 *Atgl*^{+/+} and *Atgl*^{F2A/F2A} mice (N=4 mice per group). (B) Quantification of proteins in A.
614 (C, D) The levels of FFA (C) and glycerol (D) released from gonadal WAT in chow
615 diet-fed *Atgl*^{+/+} and *Atgl*^{F2A/F2A} mice after overnight fasting (N=4-6 mice per group). (E)
616 Triglyceride hydrolase (TGH) activity in gonadal WAT from *Atgl*^{+/+} and *Atgl*^{F2A/F2A} mice
617 which were fed an HFD for 8 weeks (N=4-5 mice per group). (F, G) mRNA levels of
618 genes involved in FAO (F) and the activity of FAO (G) in gonadal WAT from *Atgl*^{+/+}
619 and *Atgl*^{F2A/F2A} mice which were fed an HFD for 8 weeks (N=3-10 mice per group). All
620 data are presented as mean±SEM. *p < 0.05, **p < 0.01.

621

622 **Figure 5. *Atgl*^{F2A/F2A} mice are resistant to diet-induced obesity.**

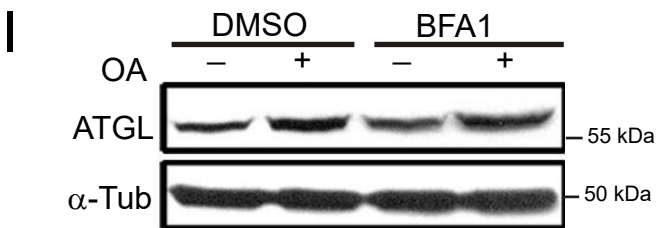
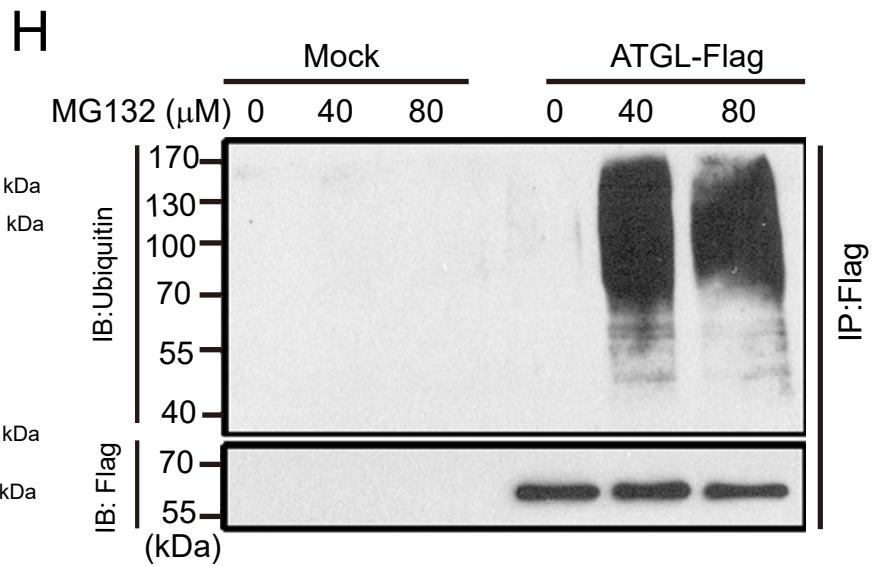
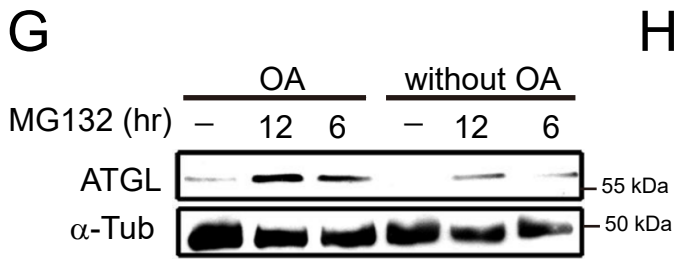
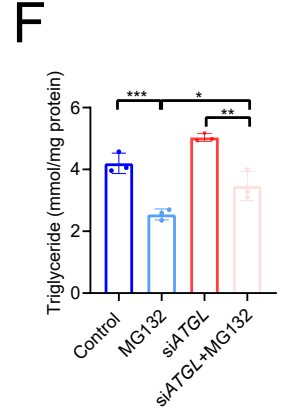
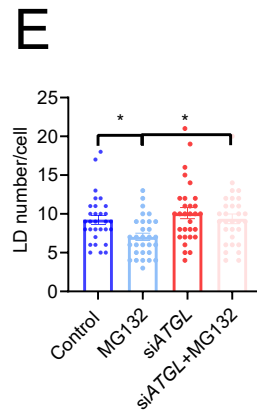
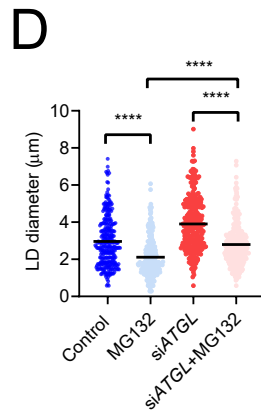
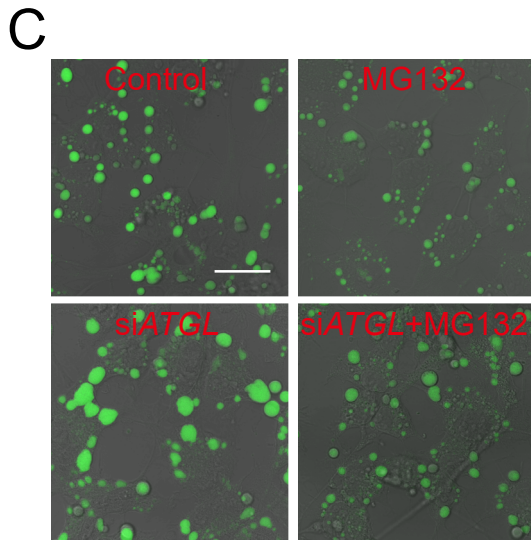
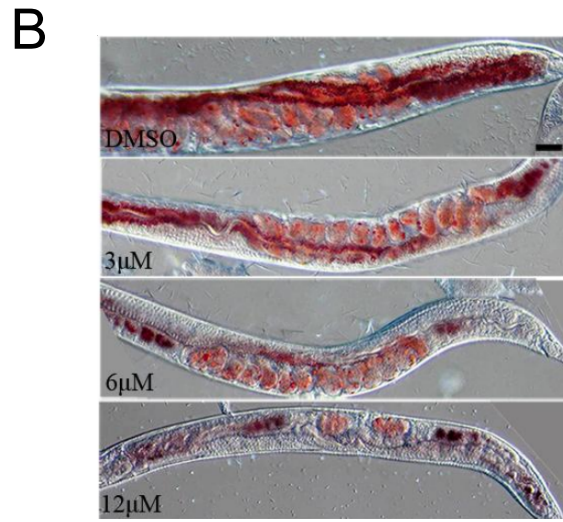
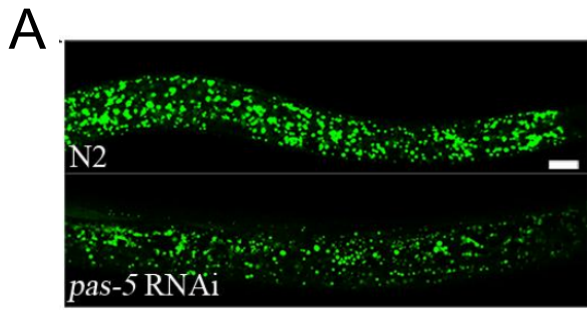
623 (A) Body weights and images (inset) of 8-week-old *Atgl*^{+/+} and *Atgl*^{F2A/F2A} mice which
624 were pair-fed an HFD for 16 weeks (N=8 mice per group). (B, C) Results of glucose
625 tolerance (B) and insulin sensitivity (C) tests after 16-week of HFD feeding (N=4-6
626 mice per group). (D) iAUC of GTT and ITT in (B) and (C). (E, F) energy expenditure in
627 HFD-fed mice (N=5 mice per group). (G) Weights of liver and different fat tissues in
628 HFD-fed mice (N=5 mice per group). (H-J) H&E staining of gonadal WAT and brown
629 adipose tissue (BAT) sections (H, scale bar 100 μm) and quantification of adipocyte
630 sizes in WAT (I) and BAT (J) in HFD-fed mice. (K) Hepatic triglyceride (left) and total

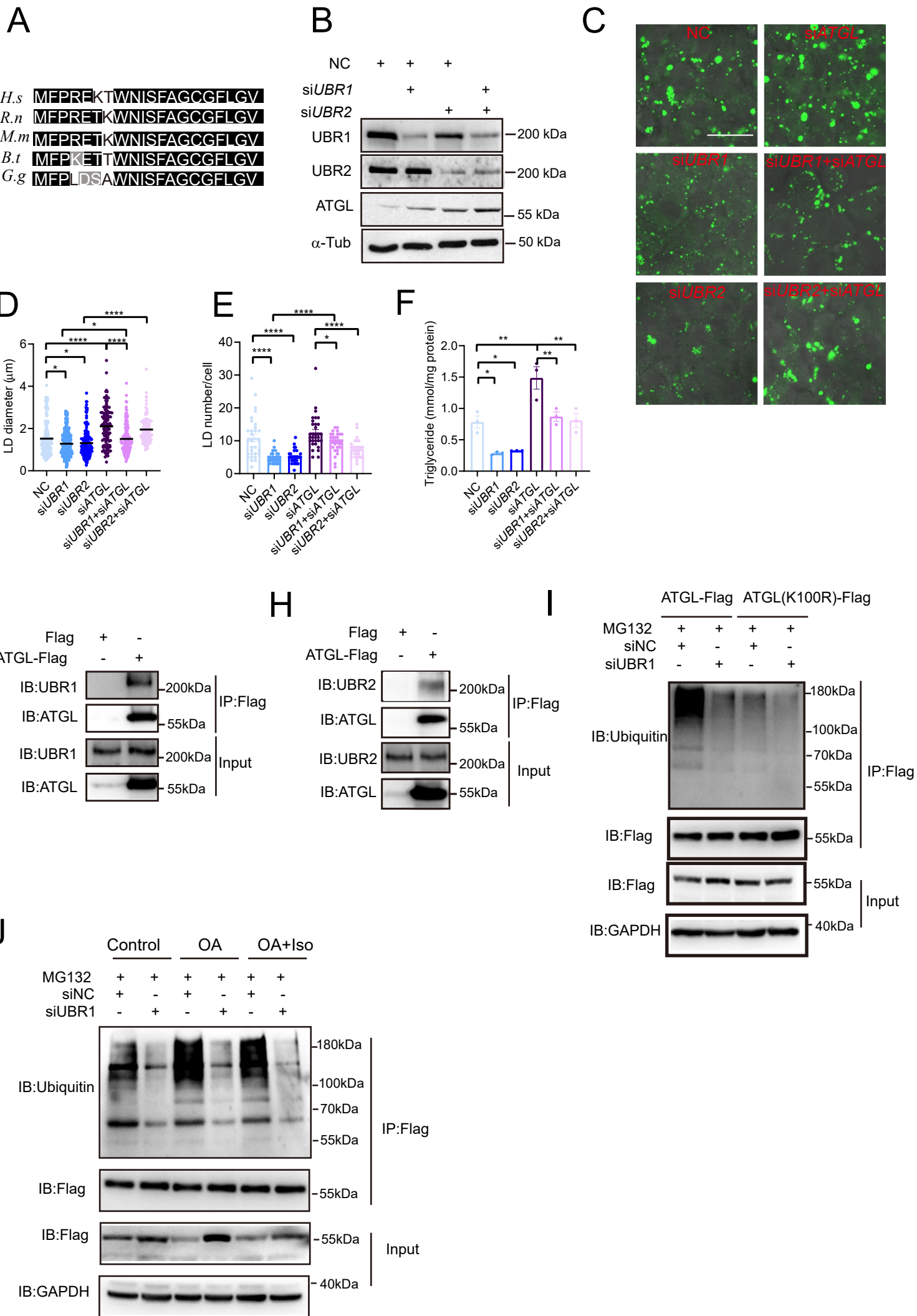
631 cholesterol levels (right) in HFD-fed mice (N=5 mice per group). (L) H&E staining of
632 liver sections from HFD-fed mice (scale bar 100 μ m). (M) Plasma ALT levels in HFD-
633 fed mice (N=4 mice per group). (N, O) mRNA levels of genes involved in FAO (N) and
634 the activity of FAO (O) in the liver from HFD-fed mice (N=4-6 mice per group). All
635 data are presented as mean \pm SEM. *p < 0.05, **p < 0.01.

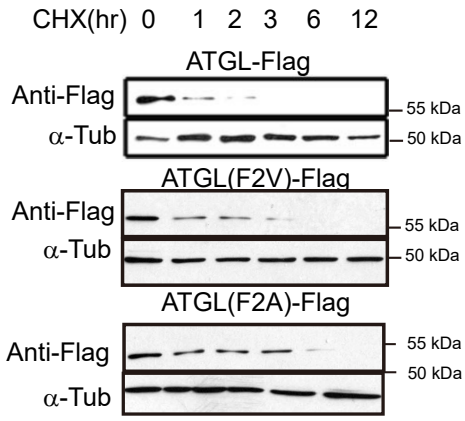
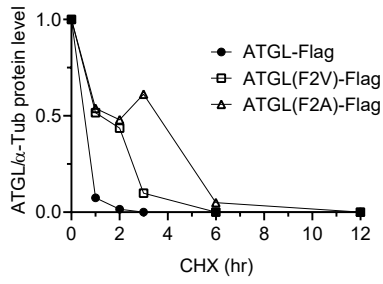
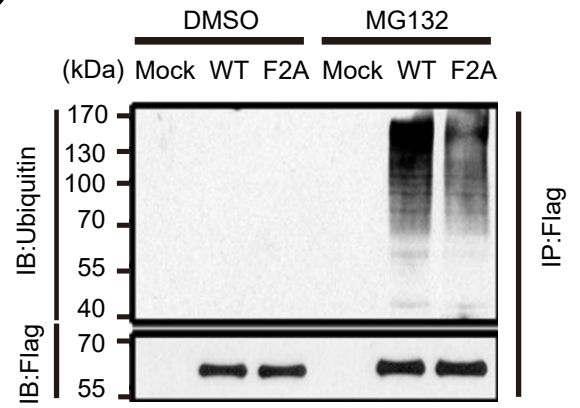
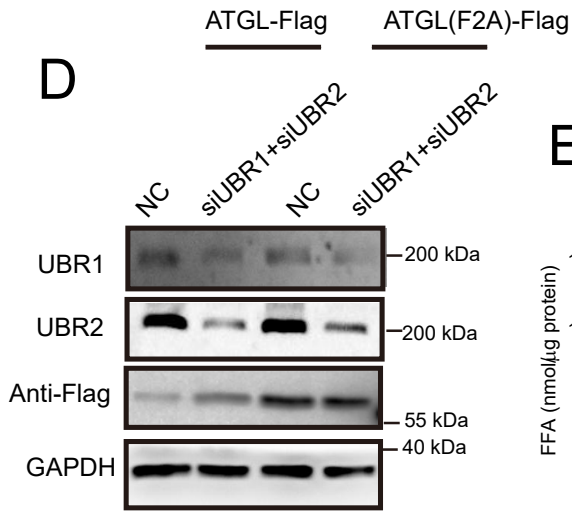
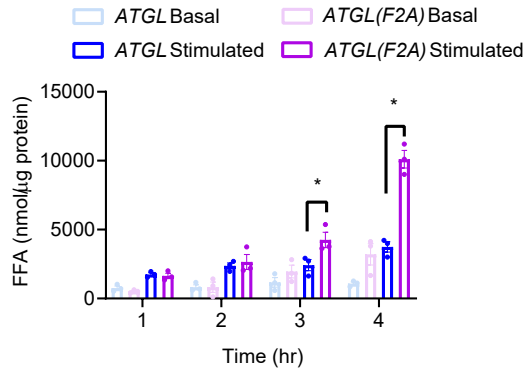
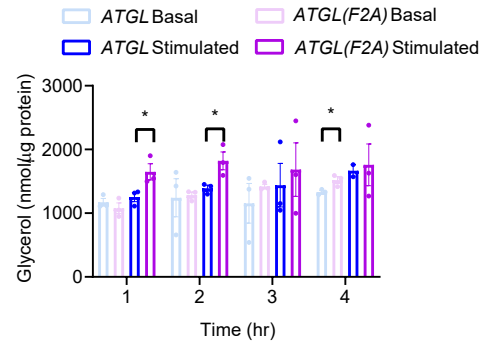
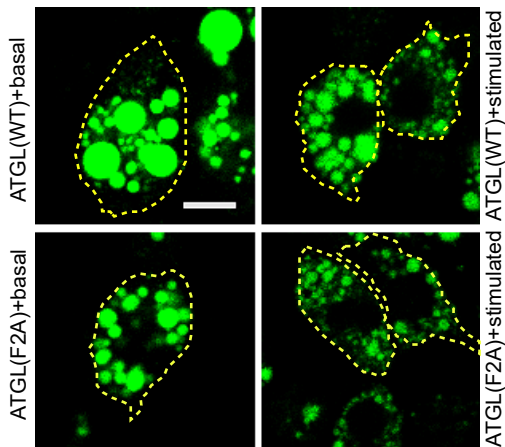
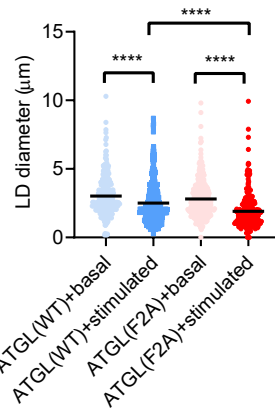
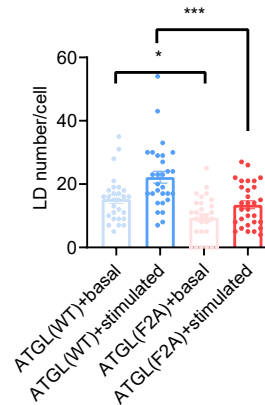
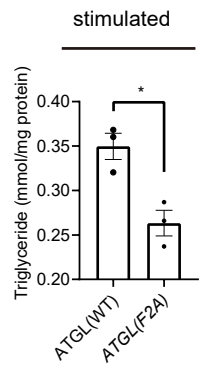
636

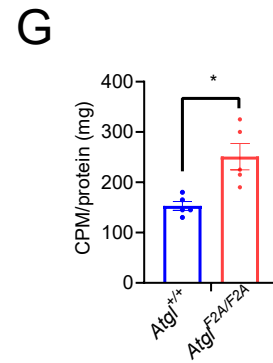
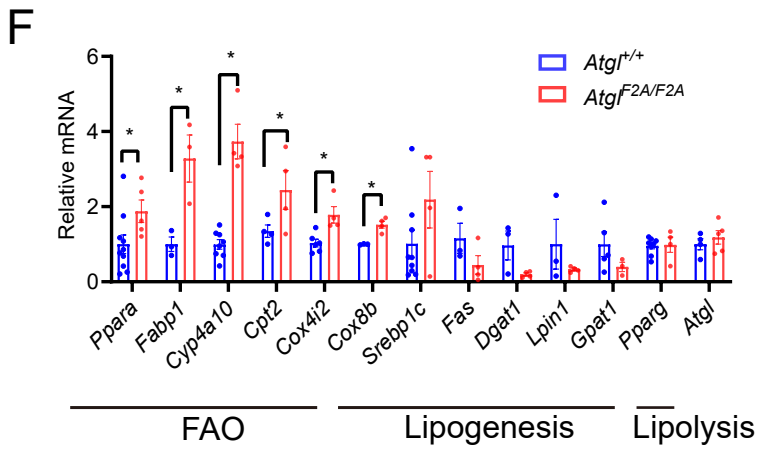
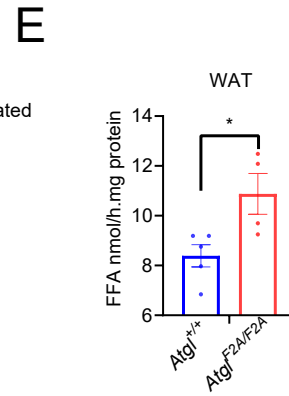
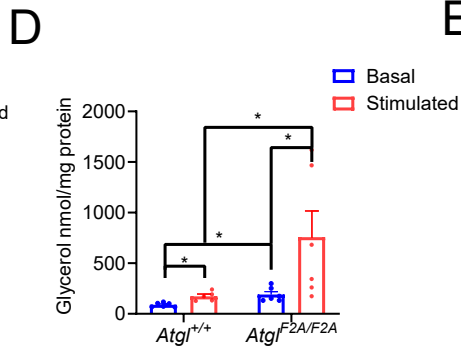
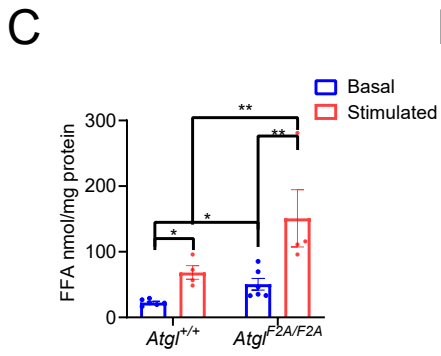
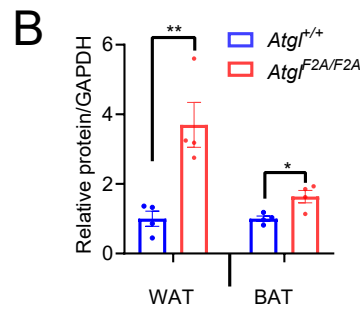
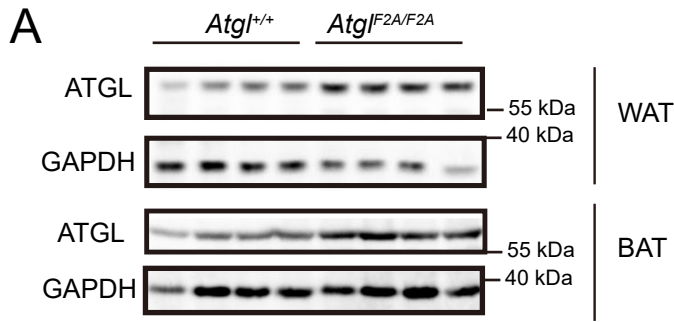
637 **Figure 6. Hepatic knockdown of UBR1 attenuates HFD-induced hepatic steatosis.**

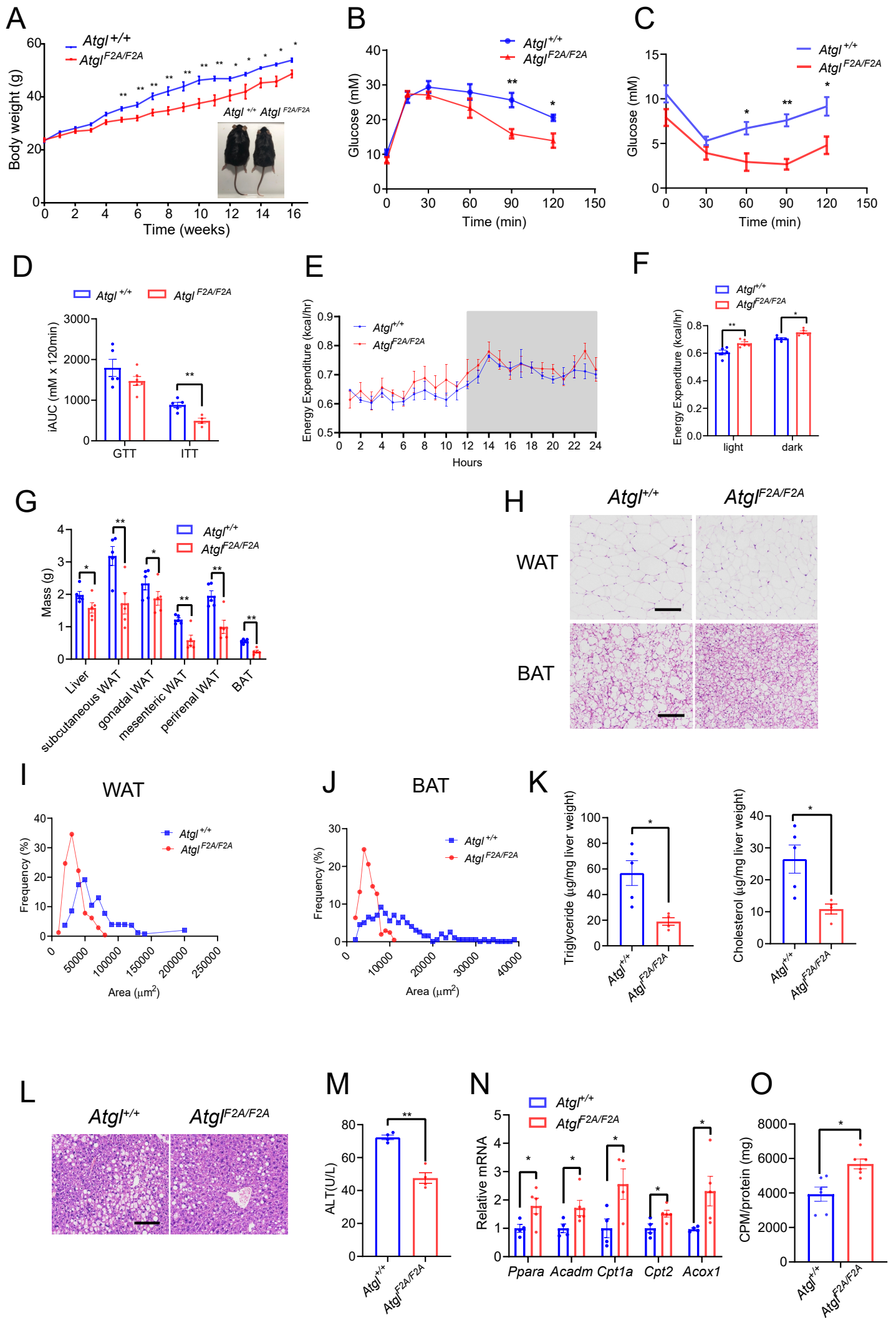
638 (A) Body weights of 8-week-old *Atgl*^{+/+} and *Atgl*^{F2A/F2A} mice injected with AAV-TBG-
639 sh*Con* or AAV-TBG-sh*Ubr1* and fed an HFD for 8 weeks (N=8 mice per group). (B, C)
640 Hepatic TAG levels (B) and plasma ALT levels (C) in HFD-fed mice (N=5 mice per
641 group). (D, E) Results of GTT (D) and ITT (E) in HFD-fed mice (N=5-6 mice per
642 group). (F) iAUC of GTT and ITT in (B) and (C). (G) Western blot analysis of proteins
643 from the liver of HFD-fed mice which were fasted for 12 hours and injected with 1 U/kg
644 insulin (i.p.). (H) mRNA levels of genes in the liver of HFD-fed mice (N=4-6 mice per
645 group). (I) Western blot analysis of proteins in the liver of HFD-fed mice (N=3 mice per
646 group). (J) Immunoprecipitation of ATGL and western blot analysis of
647 polyubiquitination levels of ATGL in liver lysates from *Atgl*^{+/+} mice infected with AAV-
648 TBG-sh*Con* or AAV-TBG-sh*Ubr1*. Results from two sh*Con*- and two sh*Ubr1*-treated
649 mice are shown. (K) Western blot detection of ATGL and UBR1 in the adipose tissue of
650 8-week-old C57BL/6 or *ob/ob* mice (N=3 mice per group). *p < 0.05, **p < 0.01, ***p <
651 0.001. For E and F, * represents *Atgl*^{+/+} + sh*Con* vs *Atgl*^{F2A/F2A} + sh*Con*; # represents
652 *Atgl*^{+/+} + sh*Con* vs *Atgl*^{+/+} + sh*Ubr1*; \$ represents *Atgl*^{F2A/F2A} + sh*Con* vs *Atgl*^{F2A/F2A} +
653 sh*Ubr1*.

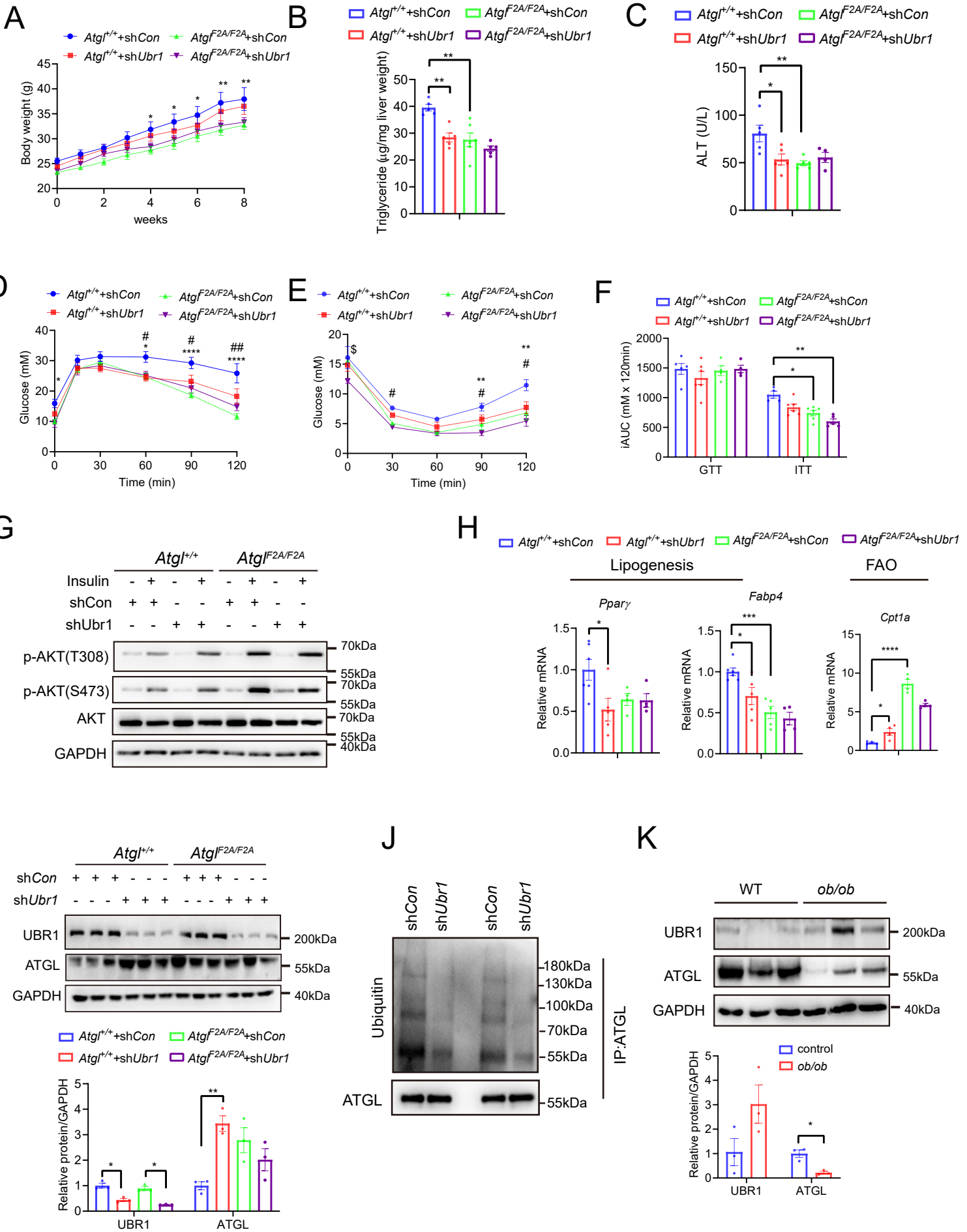


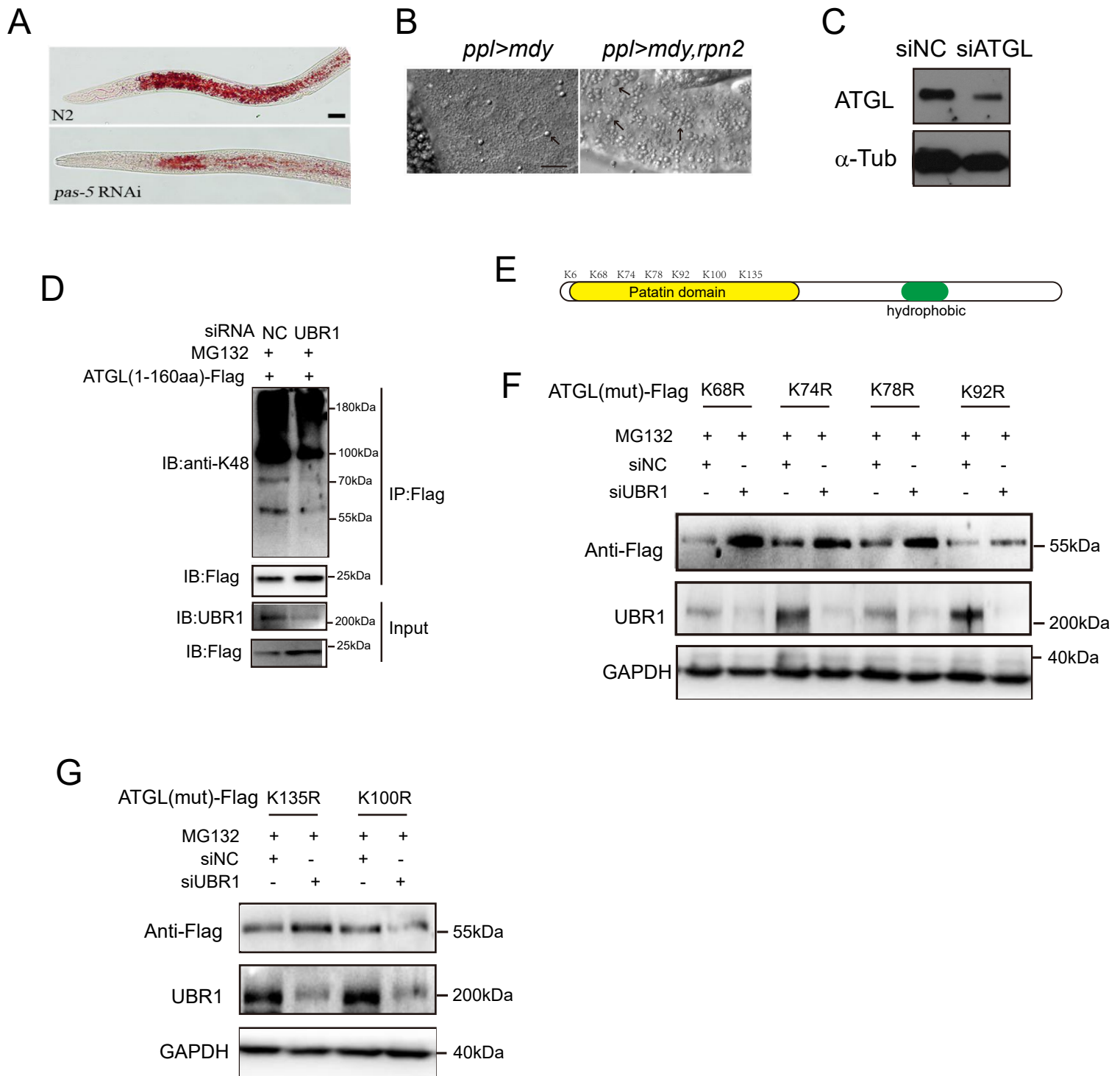


A**B****C****D****E****F****G****H****I****J**



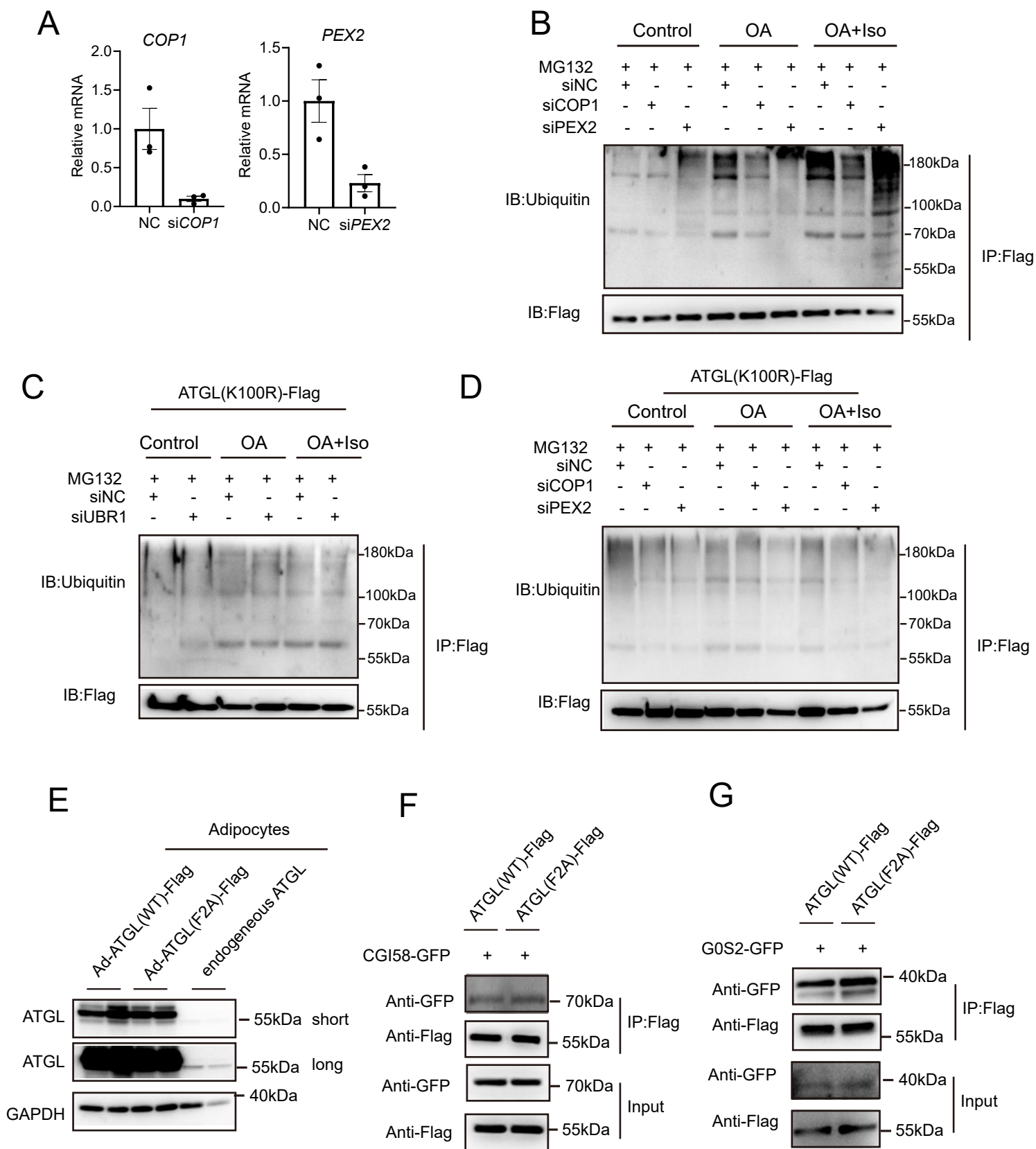






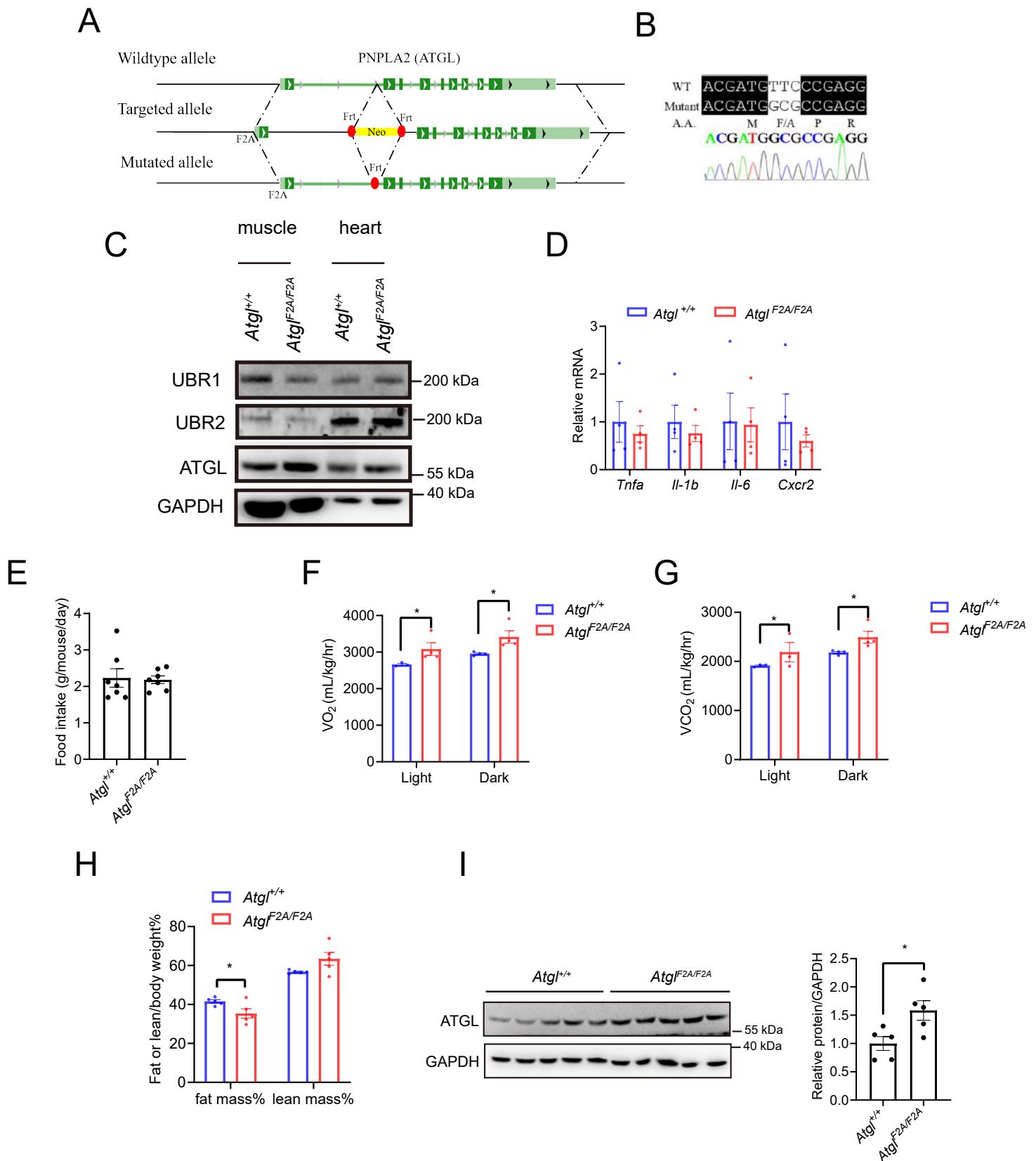
Supplemental Fig. 1 N-end rule regulation of ATGL

(A) Oil-Red-O staining for lipid droplets in *C. elegans* treated by *pas-5* RNAi compared to the N2 negative control (scale bar represents 40 μ m). (B) DIC images of lipid droplets in the 3rd instar salivary gland in fruit fly. *ppl>mdy*: overexpression of DGAT1 in salivary gland; *ppl>mdy, rpn2*: overexpression of DGAT1 and proteasome subunit Rpn2 in salivary gland (arrows indicate lipid droplets, scale bar represents 25 μ m). (C) Western blot analysis of proteins in HeLa cells transfected with indicated siRNAs. (D) Immunoprecipitation of ATGL(1-160aa)-Flag truncated protein and western blot analysis of ubiquitin in HeLa cells transfected with ATGL(1-160aa)-Flag and the indicated siRNAs. Cells were treated with MG132 for 12 hours. (E) The lysine residues in the N-terminal region of the ATGL protein. (F-G) Western blot analysis of proteins in HeLa cells transfected with ATGL(mut)-Flag vector and siRNA. Cells were treated with MG132 for 12 hours.



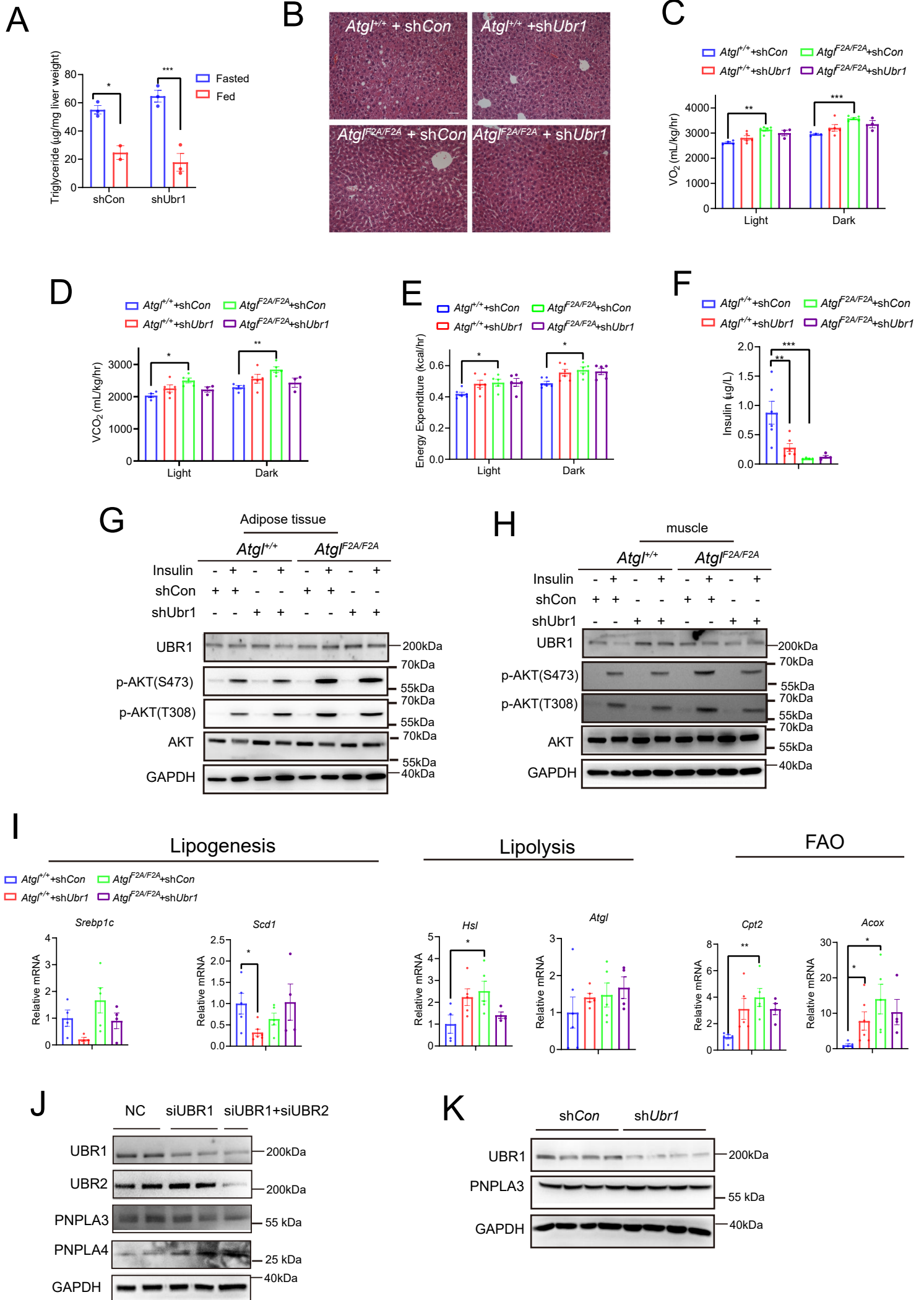
Supplemental Fig. 2 Regulation of the polyubiquitination levels of ATGL

(A) mRNA levels of COP1 and PEX2 in HeLa cells transfected with indicated siRNAs. (B) Immunoprecipitation of ATGL-Flag and western blot analysis of the polyubiquitination levels of ATGL in HeLa cells transfected with indicated siRNAs and treated with or without 100 μ M OA for 16 hours or with 100 μ M OA for 16 hours followed by ISO (0.25 mM IBMX/1 μ M isoproterenol) for 8 hours. (C-D) Immunoprecipitation of ATGL(K100R)-Flag and western blot analysis of the polyubiquitination levels of ATGL(K100R) in HeLa cells transfected with indicated siRNAs and treated with or without 100 μ M OA for 16 hours or with 100 μ M OA for 16 hours followed by ISO (0.25 mM IBMX/1 μ M isoproterenol) for 8 hours. (E) Western blot analysis of proteins in differentiated 3T3L1 adipocytes infected with equal amounts of Ad-ATGL-Flag or Ad-ATGL(F2A)-Flag. (F-G) Immunoprecipitation of ATGL(WT)-Flag or ATGL(F2A)-Flag and western blot analysis of associated proteins. All data are presented as mean \pm SEM.



Supplemental Fig. 3 Characterization of *Atgl*^{F2A/F2A} mice.

(A) Schematic illustration of the *Atgl*^{+/+} and *Atgl*^{F2A/F2A} alleles. (B) Comparison of the *Atgl*^{+/+} and *Atgl*^{F2A/F2A} sequences. In the mutant allele, the second codon is changed from F (TTC) to A (GCG). (C) Western blot analysis of proteins in the muscle and heart from *Atgl*^{+/+} and *Atgl*^{F2A/F2A} mice. (D) mRNA levels of inflammation genes in the adipose tissues from *Atgl*^{+/+} and *Atgl*^{F2A/F2A} mice which were fed an HFD for 8 weeks (N=4 mice per group). (E) Food intake in 8-week-old *Atgl*^{+/+} and *Atgl*^{F2A/F2A} mice which were pair-fed an HFD for 16 weeks (N=7 mice per group). (F-G) Oxygen consumption (VO₂) (F) and carbon dioxide production (VCO₂) (G) in HFD-fed *Atgl*^{+/+} and *Atgl*^{F2A/F2A} mice (N=3-4 mice per group). (H) Body composition of *Atgl*^{+/+} and *Atgl*^{F2A/F2A} mice which were fed an HFD for 8 weeks (N=5 mice per group). (I) Western blot analysis of ATGL in the liver of chow-fed mice (N=5 mice per group). All data are presented as mean±SEM. * p < 0.05.



Supplemental Fig. 4 Knockdown of Ubr1 suppresses HFD-induced hepatic steatosis dependent on the activity of ATGL.

(A) 8-week-old C57BL/6 mice were injected with AAV-TBG-sh*Con* or AAV-TBG-sh*Ubr1* and fed a chow diet for 1 month. Hepatic TAG levels were measured in fed or 16-hr fasted mice (N=2-3 mice per group). (B) H&E staining of liver sections from HFD-fed *Atgl*^{+/+} and *Atgl*^{F2A/F2A} mice injected with AAV-TBG-sh*Con* or AAV-TBG-sh*Ubr1*. (C-E) The oxygen consumption (C), CO₂ production (D), and energy expenditure (E) in 8-week-old *Atgl*^{+/+} and *Atgl*^{F2A/F2A} mice injected with AAV-TBG-sh*Con* or AAV-TBG-sh*Ubr1* and fed an HFD for 8 weeks (N=3-6 mice per group). (F) Plasma insulin levels in 8-week-old *Atgl*^{+/+} and *Atgl*^{F2A/F2A} mice injected with AAV-TBG-sh*Con* or AAV-TBG-sh*Ubr1* and fed an HFD for 8 weeks (N=4-6 mice per group). (G, H) Western blot analysis of proteins from the liver of HFD-fed mice which were fasted for 12 hours and injected with 1 U/kg insulin (i.p.). (I) mRNA levels of genes in lipogenesis, lipolysis, and FAO in 8-week-old *Atgl*^{+/+} and *Atgl*^{F2A/F2A} mice injected with AAV-TBG-sh*Con* or AAV-TBG-sh*Ubr1* and fed an HFD for 8 weeks (N=4-6 mice per group). (J) Western blot analysis of proteins in HeLa cells transfected with indicated siRNAs. (K) Western blot analysis of proteins in *Atgl*^{+/+} mice injected with AAV-TBG-sh*Con* or AAV-TBG-sh*Ubr1* and fed an HFD for 8 weeks. * p < 0.05, ** p < 0.01, *** p < 0.001.

Supplementary Table S1: Lipid storage phenotypes caused by RNAi knockdown of genes encoding proteasome components in *C. elegans*

Gene function		Gene name	phenotype
Proteasome core subunit	Alpha	<i>pas-1</i>	nd
		<i>pas-2</i>	nd
		<i>pas-3</i>	nd
		<i>pas-4</i>	---
		<i>pas-5</i>	---
		<i>pas-6</i>	-
		<i>pas-7</i>	nd
	Beta	<i>pbs-1</i>	---
		<i>pbs-2</i>	---
		<i>pbs-3</i>	nd
		<i>pbs-4</i>	--
		<i>pbs-5</i>	-
		<i>pbs-6</i>	---
		<i>pbs-7</i>	-
Proteasome regulatory particle	Non ATPase-like	<i>rpn-1</i>	-
		<i>rpn-2</i>	nd
		<i>rpn-3</i>	--
		<i>rpn-4</i>	-
		<i>rpn-5</i>	normal
		<i>rpn-6.1</i>	---
		<i>rpn-6.2</i>	normal
		<i>rpn-7</i>	--
		<i>rpn-8</i>	--
		<i>rpn-9</i>	nd
		<i>rpn-10</i>	normal
		<i>rpn-11</i>	-
	<i>rpn-12</i>	nd	
	ATPase-like	<i>rpt-1</i>	--
		<i>rpt-2</i>	-
		<i>rpt-3</i>	normal
		<i>rpt-4</i>	normal
		<i>rpt-5</i>	--
<i>rpt-6</i>		nd	

Lipid storage phenotypes were evaluated using PLIN-1::GFP (Liu et al., 2014). ---, -- and - stand

for severe, medium and mild reduction, respectively, in lipid storage compared to control worms.
nd, not determined.

Supplementary Table S2: Metabolic profile of *Atgl*^{+/+} and *Atgl*^{F2A/F2A} mice under chow diet.

	<i>Atgl</i> ^{+/+}	<i>Atgl</i> ^{F2A/F2A}
Body weight	23.45±0.56	23.77±0.78
Plasma triglyceride	60.19±4.84	72.69±4.81
Plasma cholesterol	83.08±2.92	72.98±4.82
Plasma glucose	9.06±1.67	7.57±0.75
Plasma insulin	0.19±0.033	0.13±0.027
Plasma FFA (fed)	0.12±0.0098	0.15±0.019
Plasma FFA (fasted overnight)	1.38±0.13	1.90±0.13 *
Hepatic triglyceride	9.92±1.28	9.62±0.77
Hepatic cholesterol	5.08±0.64	4.93±0.36

* p<0.05

Supplementary Table S3: Plasma parameters in HFD-fed *Atgl*^{+/+} and *Atgl*^{F2A/F2A} mice.

	<i>Atgl</i> ^{+/+}	<i>Atgl</i> ^{F2A/F2A}
Plasma triglyceride	50.25±5.13	55.83±5.97
Plasma cholesterol	170.51±23.06	189.79±18.28
Glucose	8.11±1.35	7.27±0.56
Insulin	2.60±0.76	0.87±0.098*
FFA	0.46±0.0088	0.56±0.034*
Adiponectin	10.39±1.48	9.48±0.99
Leptin (fold change)	1±0.37	0.78±0.17

* p<0.05

Supplementary Table S4: siRNA sequences

siRNA	sense (5'-3')	antisense (5'-3')
human UBR1	5' - GGCGUUGAGUCUUCGAUUATT- 3'	5'- UAAUCGAAGACUCAACGCCTT- 3'
human UBR2	5' - GCCGCUUUGAACUUUAUCATT- 3'	5'- UGAUAAAGUUCAAAAGCGGCTT- 3'
human ATGL	5' - CGGCGAGAAUGUCAUUUAUATT- 3'	5'- UAUAAUGACAUUCUCGCCGTT- 3'
human PEX2	5'- GCUAGUUUGGUCCAGUUUTT- 3'	5'- AAACUGGGACCAAACUAGCTT- 3'
human COP1	5'- GCUGUGGUCUACCAAUCUATT- 3'	5'- UAGAUUGGUAGACCACAGCTT- 3'